Organic Photovoltaic Devices: Atmospheric Fabrication and Characterization

A Thesis Submitted to the
College of Graduate Studies and Research
in Partial Fulfillment of the Requirements
for the degree of Master of Science
in the Department of Physics & Engineering Physics
University of Saskatchewan
Saskatoon

By
Robert Paul Christian Bauer

Permission to Use

In presenting this thesis in partial fulfilment of the requirements for a Postgraduate degree from the University of Saskatchewan, I agree that the Libraries of this University may make it freely available for inspection. I further agree that permission for copying of this thesis in any manner, in whole or in part, for scholarly purposes may be granted by the professor or professors who supervised my thesis work or, in their absence, by the Head of the Department or the Dean of the College in which my thesis work was done. It is understood that any copying or publication or use of this thesis or parts thereof for financial gain shall not be allowed without my written permission. It is also understood that due recognition shall be given to me and to the University of Saskatchewan in any scholarly use which may be made of any material in my thesis.

Requests for permission to copy or to make other use of material in this thesis in whole or part should be addressed to:

Head of the Department of Physics & Engineering Physics
53 Physics Building
116 Science Place
University of Saskatchewan
Saskatoon, Saskatchewan
Canada
S7N 5E2

Abstract

Organic electronics show promise as a future alternative to crystalline inorganic semiconductors in a variety of applications, with advantages in flexibility, and fabrication cost. Organic photovoltaic devices are one such application with a growing demand for clean energy, solar energy has the possibility to fill a large portion of the demand. This thesis focuses on the fabrication and testing of organic photovoltaic devices in ambient conditions, from initial device fabrication to manipulation of device structure to invert the flow of electrons, ending with a small look at the change in device function while exposed to simulated solar illumination.

The theory of photovoltaic devices and properties of organic electronic materials are the basis of device design. Considering the competing factors of charge transport, recombination and absorption, devises can be designed to operate within a reasonable efficiency. To improve device function degradation and device limiting factors must be considered and rectified.

Device fabrication utilized two basic techniques spin coating for all organic materials and physical vapor deposition for inorganic materials. A single set of acceptor donor absorption pair were utilized, with three different buffer materials, and two different metals for contacts. These materials were combined in a simple planar bulk heterojunction architecture. Standard device testing methods were employed to ensure valid comparison with reported results.

Initial devices failed due to a variety of factors, from shorts in the devices caused by insufficient cleaning of substrates to destruction of devices due to testing apparatus. Rectifying these problems resulted in devices having power conversion efficiencies as high as 3.23% using a material that is not expected to exceed 5%. Manipulation of device structure by substitution of materials confirmed device design principles, including the inversion of device current flow by changing the buffer materials. Changes in device function due to exposure to solar illumination over a short period were investigated, yielding mixed results dependent on the initial state of the device.

Acknowledgements

Many people have contributed to the success of this research. First i would like to thank my supervisors Professors Gap Soo Chang and Ramaswami Sammynaiken with out whom this project would not have been possible, they provided both the means and guidance required for success. I would also like to thank the members of my commitee Professors John Tse, Yansun Yao, Seok-Bum Ko and my commitee chair Professor Kaori Tanaka.

I would like to thank my group members past and present for their insights, inspiration and support. In particular I would like to acknowledge, and thank, Miguel Young for his contribution to this research, during his summer with our group we made a variety of devices testing various aspects of device structures. I would also like to thank Dr. John Purdy for his insights into solving the surface energy problem.

There are many people who aided in the research in supporting roles. I would like to thank Marj Granrude and Debbie Gjertsen for helping in countless ways, many of which i will never know. The shop staff in Physics always willing to lend a hand or tool when equiptment was not working quite right, Blair Chomyshen, Ted Toporowski and Jill Cornish. There are many more people to thank, as with any project it takes many people to have success.

Finally I would like to thank my family and freinds whos support was invaluble throughout the ups and downs of the research process.

Dedicated to my fiancée who encouraged me throughout this project.

Contents

List of Tables

List of Figures

List of Symbols and Abbreviations

EU	European Union
ISS	International Space Station
OPV	Organic Photovoltaic
ITO	Indium Tin Oxide
NREL	National Renewable Energy Laboratory
E	Energy
ψ	Wave Function
$\hat{\boldsymbol{H}}$	Hamiltonian
n	Principle Quantum Number
l	Orbital Angular Moment Quantum Number
m_l	Magnetic Quantum Number
m_s	Magnetic Spin Quantum Number
R	Radial Wave Function
Y	Spherical Harmonics Function
r	Radial Distance
θ	Polar Angle
ϕ	Azimuthal Angle
m_e	Mass of an Electron ($9.11\text{x}10^{-31} kg$)
e	Charge of an Electron ($-1.60\text{x}10^{-19} C$)
Z	Atomic Number
ϵ_o	Permittivity of Free Space ($8.85\text{x}10^{-12} F \cdot m^{-1}$)
h	Planks Constant ($6.63\text{x}10^{-34} J \cdot s$)
VB	Valence Band
CB	Conduction Band
HOMO	Highest Occupied Molecular Orbital
LUMO	Lowest Unoccupied Molecular Orbital
E_f	Fermi Energy
k	Boltzmann Constant ($1.38\text{x}10^{-23} J \cdot K^{-1}$)
T	Temperature
m_e^*	Effective Mass of an Electron
m_h^*	Effective Mass of a Hole
$\boldsymbol{H}_{SO}$	Spin-Orbit Interaction Hamiltonian Term
c	Speed of Light in a Vacuum
$\boldsymbol{s}$	Spin Vector of Electron
$\boldsymbol{L}$	Orbital Angular Momentum Vector
B	Spectral Radiance
λ	Wavelength
AM 1	Air Mass of 1 (optical path length perpendicular to the earths surface)
SMARTS	Simple Model of Radiative Transfer of Sunshine
AM 1.5	Air Mass of 1.5 (optical path length at an angle of 37^o up from the surface of the earth towards equator)
η	Refractive Index
ς	Field Reflection Coefficient
t	Field Transmission Coefficient
s	Perpendicular Polarization
p	Parallel Polarization
Θ_i	Incident Angle
Θ_t	Transmitted Angle
$\boldsymbol{E}^{(+)}$	Electric Field Vector
$\boldsymbol{H}^{(+)}$	Magnetic Field Vector

$\boldsymbol{\Upsilon}$	Transfer Matrix
$\varkappa$	Phase Shift of Transmitted Light
ϖ	Geometric Coefficient
i	Imaginary Unit
$\mathfrak{r}$	Reflection Coefficient
$\mathfrak{R}$	Reflectance
$\mathfrak{T}$	Transmittance
α	Absorption Coefficient
I	Intensity of Light
ω	Frequency
τ	Time
Λ	Area
$\hbar$	Dirac's Constant ($\frac{h}{2\pi} = 1.05\text{x}10^{-34}$)
W	Transition Probability
V	Potential Energy
U_I	Dyson Series
c_n	Perturbation Expansion
$\delta_n i$	Kronecker Delta Function
ρ	Density of States
$\mathbf{A}$	Vector Potential
$\mathbf{q}$	Wave Vector
$\mathbf{p}$	Momentum
$\bar{m}_e^*$	Reduced Effective Mass of Electron
$\mathcal{I}$	Current
$\mathcal{R}$	Resistance
ι	Device Current
$\mathcal{I}_S$	Saturation Current
V_T	Thermal Voltage
G	Conductance
V_{OC}	Open Circuit Voltage
$\mathcal{I}_{SC}$	Short Circuit Current
J	Current Density
P	Power
FF	Fill Factor
ξ	Power Conversion Efficiency
PEDOT:PSS	Poly(3,4-Ethylenedioxythiophene) Polystyrene Sulfonate
PCBM	[6,6]-Phenyl-C61-Butyric Acid Methyl Ester
P3HT	Poly(3-Hexylthiophene-2,5-Diyl)
PFN	Poly [(9,9-Bis(3'-(N,N-Dimethylamino)Propyl)-2,7-Fluorene)-Alt-2,7-(9,9Dioctylfluorene)]

Chapter 1

Introduction

1.1 Organic Electronics

Organic electronics are electronics devices that use carbon-based materials as the semiconductor in the device [1, 2]. Organic materials vary in type and structure. There are three basic types of organic materials when thinking about organic electronics. A small molecule is a structure consisting of less than roughly 1000 atoms [3]. Large molecules are non repeating molecule consisting of greater than 1000 atoms. The final classification are polymers which consist of repeating groups of atoms in a chain. The wide variety of organic materials available makes the possibilities for applications extremely vast [2]. By layering the appropriate molecules and polymers it is possible to make devices completely out of organic materials [4, 5]. Electrical characteristics of an organic semiconductor are determined by its structure, and how it interacts with surrounding molecules. Carbon is an abundant resource that can be transformed into a nearly infinite number of possible molecules with a vast array of possible applications [6]. Finding a structure that interacts well and has the desired properties is an ongoing process. Creation and testing of new organic semiconductors is rapid and out reaches the testing of these materials. There is a high demand for testing of these materials and characterization for different applications.

Characterization of organic molecules for electronic applications takes on several forms. It starts with testing during synthesis of the organic molecule to classify the molecule or polymer by size and functional groups. Chemists can selectively functionalize molecules tailoring the properties of a molecule, there are general trends that appear when functionalizing molecules [7]. Functionalization may not follow the desired trend, testing is required to investigate changes, one of the quickest methods to identify the change in electrical properties is to fabricate a device. Further testing of the fundamental properties of the material show properties of the material that can be used in the design of devices, and mechanisms of operation [8]. The mechanisms of operation are often complicated and require device fabrication to verify the practical mechanism at work in devices. Characterization of organic materials requires an array of experimental options. These insights provide possible applications of the material, and optimize device design. Large scale

production of organic materials is needed to reduce the cost of the organic devices.

Organic electronics are a growing section of the electronics market with major advancements in thin film technologies [9]. Solution processing is one of the major benefits of organic electronics, opening up low cost fabrication opportunities [10]. Fully solution-processed devices reduce the need for costly equipment required to dope inorganic semiconductors. Inorganic devices require ultra clean environments for reasonable yield and reliable devices; the inorganic materials are expensive to refine and dope, to tailor their electrical properties [11]. Organic materials do not require the same level of clean room environment and production methods are more easily scaled for large area, and rapid production. Fabrication of organic devices is done using a bottom-up approach where each successive component is added to the device, reducing the amount of material required for each device; differing from the top-down approach favored in inorganic devices. Roll to roll processing is one of the proposed scalable fabrication techniques, that is already used in large printing operations. Organic materials can be made into inks and processed in the same way. This large scale fabrication has the possibility of making smaller facilities that produce more devices than current facilities. The amorphous thin films that organic semiconductors form are not greatly affected by the stress and strain of bending and stretching.

1.2 Renewable Energy

Demand for renewable clean energy has been compounded by public interest in eco-friendly energy production [12]. Recent disasters with nuclear energy have raised fears of energies that have overt negative effects on the environment and safety of the public; have pushed renewable energy interest further. Unrest in several areas of the world, and a need to have self sustainable energy resources has shown that renewable energy, despite costly initial capital requirements, may have additional long term benefits. Climate change also contributes to the call for clean energy in the forms of solar, wind, geothermal and tidal. The wide variety of renewable energy sources allows for a diverse power system, with smaller local systems contributing to the overall power need [13]. Micro-grid systems can reduce the fragile nature of current macro system, reducing the possibility of large scale blackouts. Several nations have lofty renewable energy goals with the European Union (EU) having a minimum goal of 20% by 2020; and some members aiming for 40 % [14], Iceland is nearly 100% powered by geothermal and hydro [15].

Solar energy has been used for centuries for many applications from growing crops to cooking food. In 1954 Daryl Chapin, Gerald Peterson, and Calvin Fuller, from Bell Laboratory developed the first silicon solar cell [1]. The solar power incident on the earth on a daily basis could supply a large portion of our energy needs if harnessed [16]. Recently solar power has become viable for individuals even inside populated areas; providing

the possibility to make a profit by selling power back into the grid. Solar city has started solar leasing where one can lease the solar power system, paying fixed rates for power by providing a roof for the system. Large scale solar projects have been started all over the world in an effort to reduce reliance on coal, petroleum, and nuclear power. With the push for space exploration solar energy proved revolutionary, Vanguard being the first satellite equipped with solar panels [1]. Space technology has favored solar energy over the nuclear alternative for satellite systems, including the International Space Station (ISS), where the proximity to the sun allows these lower cost alternatives to shine. Combining low cost solar cells with rechargeable batteries, has replaced the need for costly regular replacement of batteries in warning systems; for several industries in remote locations. Solar panels also provide power to remote communities in developing countries.

The current organic photovoltaic (OPV) cell structure has been around since 1994 when R. N. Marks *et al.* created the single layer OPV structure, based on an organic polymer between indium tin oxide (ITO) and aluminum [17]. In recent years the efficiency of OPVs has increased significantly. With dye-sensitized cells reaching 11.4% and tandem cells reaching 12% just behind amorphous silicon solar cells at 13.4%. The National Renewable Energy Laboratory (NREL) tracks solar cell efficiencies as seen in Figure 1.1 [18].

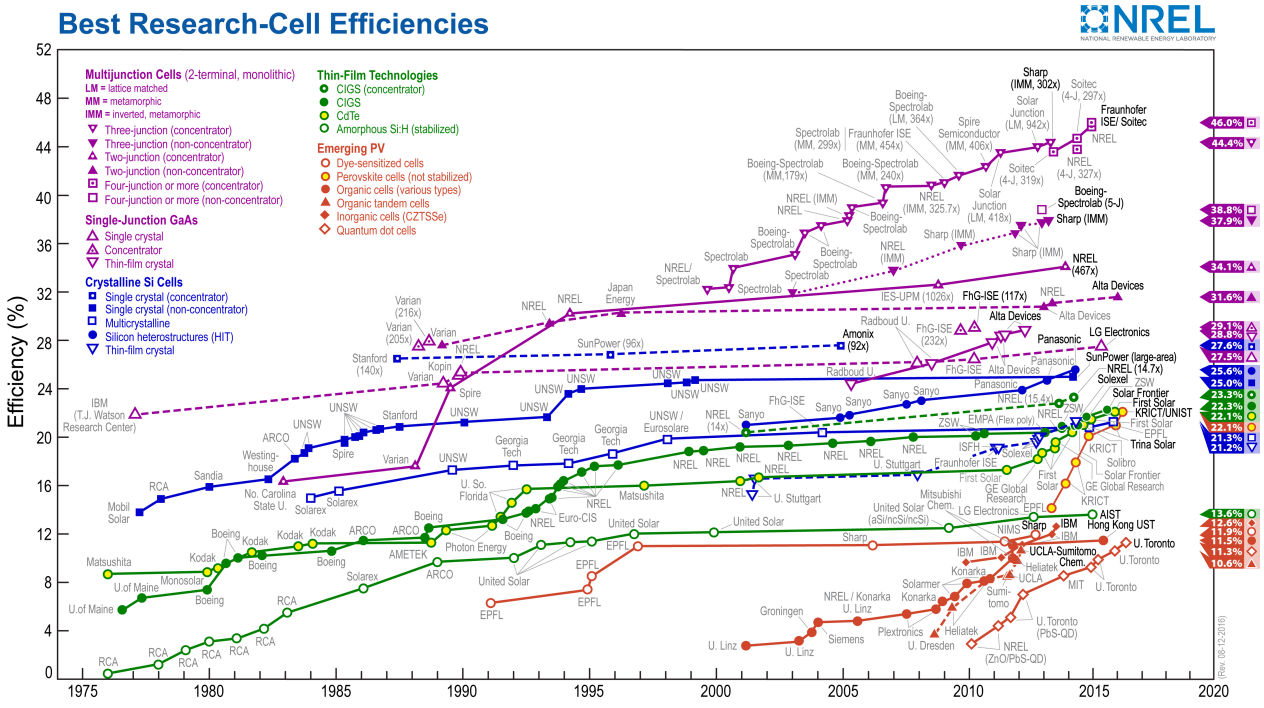

Figure 1.1: NREL best solar cell power conversion efficiency records. Courtesy of National Renewable Energy Laboratory, Golden, CO. Adapted with permission [18]

Organic photovoltaic devices benefit from the robust nature of organic electronic fabrication processes. Although the life expectancy of OPVs is relatively short when compared to the inorganic alternatives one could fabricate these devices in emergency situations with minimal equipment. Rapid fabrication for instant

use would be advantageous given the short life expectancy of organic photovoltaic devices limiting their application in large scale power generation.

1.3 Research Motivation

The aim of this project is to find a robust method to fabricate organic photovoltaic devices. Focusing on being able to fabricate devices in atmospheric conditions and being able to adapt to different materials; a true test being able to fabricate devices using a standard metric, that can be adapted to different purposes. The four goals of this project are to: first produce a standard device structure and fabrication method, second investigate the effects of changing various parts of the device structure on device performance, third reverse current flow in the device creating an inverted device standard, finally test the changes in the device performance during prolonged exposure to simulated sun light. Typical fabrication generally involves a highly controlled environment but even in an imperfect environment organic photovoltaics can be fabricated opening the door to emergency power generation. For fabrication in emergency situations the fabrication environment will be difficult to control, one may be able to limit contamination but access to a clean room would be unlikely. Looking at atmospheric influences on the fabrication process and methods to mitigate negative impacts. This is the first step toward packaging emergency solar power generation solutions.

Moving toward atmospheric fabrication of OPVs, starting from not having fabricated OPVs and not having great success within the research group fabricating OPVs. To start the project a basic fabrication method and device structure were needed and the structure and method needed to be adapted to reliably fabricate reasonable devices to attain this, a series of device fabrications were preformed working out a reasonable fabrication method. The initial fabrication method was based on published fabrication guides and augmented such that it would work with available tools. From this initial fabrication method, the back-contact mask was refined and the device design was altered to reduce recombination and increase device yield by adding an electron transport tunneling buffer layer. The initial ITO coated microscope slide device substrates were exchanged with patterned ITO substrates to improve device yield and testing. Once the fabrication method was derived then fabrication was practiced and power conversion efficiency of devices were tested. At this point the device structure optimization was attempted. Then short-life time tests of devices were preformed to look at the changes in device efficiency. To open the possibility of alternate device architectures an inverted design was investigated. The initial design removed the rear buffer layer and replaced the front buffer layer. Alternate metal contacts were tested. Then a back buffer layer was added which was the original front buffer layer. The life time of inverted devices was also tested. Finally, an alternate absorbing material mixture was employed to test the adaptability of the device design and fabrication method.

This thesis is laid out as follows:

Chapter 2 consists of a brief review of physical principals applicable to device design considerations. Then the basic principles of solar cell function are outlined highlighting major design constraints and comparing past current and prospective device designs outlining strengths and weaknesses.

Chapter 3 lays out the fabrication techniques utilized over the course of this project and process considerations used to optimize the various methods. This chapter also outlines the testing procedure and the metric upon which the devices will be evaluated.

Chapter 4 follows the research as laid out in the plan below stating the results of devices and the changes to the method based on these results, possible changes that were not preformed are also described here as a link to future work that could be done.

Chapter 5 summarizes the results of this research and future work.

Chapter 2

Theory

2.1 Orbital Structures and Electronic Properties of Organic Semiconductors

The electronic structure of organic semiconductors is affected by several properties of the film that make up the semiconductor [2]. The most basic components are the molecular orbitals on the molecule itself. Then one has to consider the solvent and other impurities in the film, if it was created using a solution processing. Finally, the stacking of the film has to be considered.

When considering electronic properties of a material one must investigate the nature of electrons in the system. Energy levels and orbital locations of electrons are important factors and can be modeled by solving the Schrödinger equation (Eq. 2.1). Where E is the energy of the electron described by the wave function ψ and $\hat{H}$ is the Hamiltonian operator that describes the energy in the system,

$$E\psi = \hat{H}\psi \tag{2.1}$$

The wave function (Eq. 2.2) provides the probable positions of electron's orbital state, can be spared into two functions a radial wave function R and a spherical harmonic function Y, based on a set of four quantum numbers; n the principle quantum number, l the orbital angular moment quantum number, m_l the magnetic quantum number and m_s the spin magnetic quantum number [19, 20].

$$\psi_{n,l,m_l}(r,\theta,\phi) = R_{n,l}(r)Y_{l,m_l}(\theta,\phi) \tag{2.2}$$

By solving the Schrödinger equation for a single hydrogen atom, using the wave function one finds the energy eigenvalues (Eq. 2.3) for the states given by the wave equation [20]. Where m_e is the mass of an electron, e is the charge of an electron, Z is the atomic number, ϵ_o is the permittivity of free space, and h is planks constant. This function is given in spherical coordinates so r is the radial distance, θ is the polar angle and

ϕ is the azimuthal angle.

$$E_n = -\frac{m_e e^4 Z^2}{8\epsilon_o^2 h^2 n^2} \tag{2.3}$$

Using these energy levels one can make a picture of the energy separation of the eigenstates displayed in Figure 2.1.

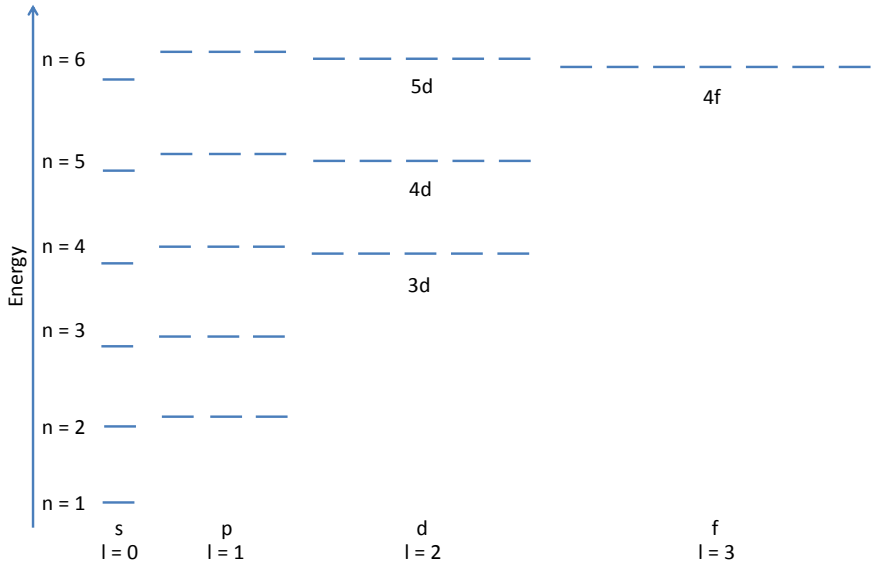

Figure 2.1: Diagram of atomic energy levels with respect to quantum numbers

Selection rules given in Eqs. 2.4 and 2.5 one can estimate the energy transitions for absorption and emission experiments [20].

$$\Delta l = \pm 1 \tag{2.4}$$

$$\Delta m_l = \begin{cases} 0 \\ \pm 1 \end{cases} \tag{2.5}$$

Molecular orbitals are formed by the bonding of two adjacent atoms. The formation of molecular orbitals causes the atomic orbitals to shift into bonding and anti-bonding orbitals; anti-bonding orbitals are denoted with a superscript star as seen in Figure 2.2 [21, 20]. The shift of the energy levels results in a broadening of the energy states and orbital shape. Hybridization of atomic orbitals allows for a change in the orbital shape, thus a change in the bond angles.

If a large crystal is formed where the atoms are bonding with multiple surrounding atoms this broadening can be significant leading to the overlap of orbitals. This is typical in crystalline systems and due to the density of broadened states, the orbitals tend to overlap thus the states form bands. There can be gaps in

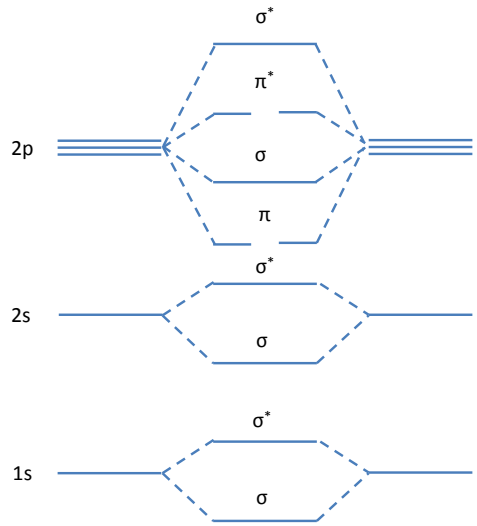

Figure 2.2: Diagram of molecular Orbitals showing the broadening of energy levels due to bonding of atoms. This is a special case for certain diatomic molecules where the π^* has a lower energy than the σ^* orbital. [21]

the bands which is used to classify types of materials into either conductors, semiconductors or insulators. There are two general bands in systems that have a band gap: the occupied band also called the valence band (VB) and the unoccupied band or conduction band (CB) [20]. Conductors are materials where there is no band gap, therefore electrons are easily excited from occupied states into unoccupied states with minimal energy. Semiconductors have a band gap that can be overcome with a moderate input energy. Insulators have very large band gaps and require a very large amount of energy to excite electrons from the valence band to the conduction band.

In molecular systems the states are not as broad as in crystalline systems, thus the states of an individual molecule can be considered to be discrete localized states similar to that of a dopant in a crystalline lattice. To show this difference the energy levels within a molecular system are called molecular orbitals, with analogies to a crystalline system. The last occupied state in a molecular system is called the highest occupied molecular orbital (HOMO), and the first unoccupied state is called the lowest unoccupied molecular orbital (LUMO); which are similar to the end of the valence band and onset of the conduction band [21]. The gap between occupied and unoccupied states in a molecular system defines an energy gap.

The Fermi level is the energy of the last occupied state at absolute zero. The Fermi energy can be more useful as it denotes the highest occupied state at a given temperature seen in Eq. 2.6 for conductors, and Eq. 2.7 [20]. The Fermi energy (E_f) in semiconductors generally lies with the energy gap due to thermal

excitation of charge carriers into previously unoccupied states. When aligning the energy diagrams of two adjacent materials one aligns them to have matching Fermi energies.

$$E_{f_{conductors}}(T) = E_{fo}\left[1 - \frac{\pi^2}{12}\left(\frac{kT}{E_{fo}}\right)\right] \tag{2.6}$$

$$E_{f_{semiconductors}}(T) = \frac{E_{gap}}{2} + \frac{3kT}{4} ln\left(\frac{m_h^*}{m_e^*}\right) \tag{2.7}$$

where m_h^* is the effective mass of a hole and m_e^* is the effective mass of an electron.

Ionization of a material is done by removing electrons from a material. The work function is the difference in energy between the vacuum level and the Fermi energy. The vacuum level is the point at which electrons are no longer bound to their respective atom, there are states within the vacuum level but they are unbound states [20]. Electrons in the material close enough to the surface to the sample can leave if they are not scattered by other sub-atomic particles in the system.

Types of excited electronic states in organic materials are a major consideration for device design. There are three states that an electron can occupy: singlet, doublet and triplet [22]. Singlet states have a spin of 0, 0 angular momentum and are generally referred to using the following equation.

$$\mid 00\rangle = \frac{1}{\sqrt{2}}\left(\uparrow\downarrow - \downarrow\uparrow\right) \tag{2.8}$$

Doublet states have a total electron spin quantum number of $\pm\frac{1}{2}$, this is seen mainly in free radicals; a molecule with a single unpaired electron. Triplet states have a spin of 1 and an angular momentum of either ± 1 or 0, having three general states typically shown by Eq. 2.9 [23].

$$\begin{aligned} \mid 11\rangle &= \uparrow\uparrow \\ \mid 10\rangle &= \tfrac{1}{\sqrt{2}}(\uparrow\downarrow + \downarrow\uparrow) \\ \mid 11\rangle &= \downarrow\downarrow \end{aligned} \tag{2.9}$$

The doublet excited state is typically a charged system resulting in a non-integer spin of one half. Singlet excited states have the paired electrons of opposite spin in phase, triplet excited states have spin of either the same orientation or out of phase. These states occupy different energy levels, singlet states are typically responsible for bonding, and triplet for anti-bonding. This generally means the first excited triplet state is at a lower energy than the first excited singlet state. The difference in spin orientation and phase makes movement of electrons between the different types of excited states forbidden transitions. Combining the lower energy and lower probability of recombination of triplet excited states, results in the general distribution

of excited states in organic materials of 3:1 triplet to singlet excited states [24].

Charge transport in a system is governed by the carrier lifetime, diffusion rate, and charge carrier mobility. The distance a carrier can travel is determined by the mean free path of the charge carrier. If the charge carrier interacts with an atom it will lose energy to the atom. The nature of the charge carrier determines its mobility and lifetime. Charge carriers in the triplet states tend to have a lower mobility than that of single state carriers but they have a longer lifetime resulting in larger diffusion lengths on the order of 10 nm [25].

Spin-orbit interaction is the interaction of the spin of the electron with the angular momentum of the orbital, which can be described by Eq. 2.10 [26].

$$\boldsymbol{H}_{SO} = \frac{Ze^2}{2m_e^2c^2r^3}\boldsymbol{s}\cdot\boldsymbol{L} \tag{2.10}$$

where $\boldsymbol{H}_{SO}$ is the spin-orbit interaction Hamiltonian, c is the speed of light in a vacuum, $\boldsymbol{s}$ is the spin vector of the electron, and $\boldsymbol{L}$ is the orbital angular momentum vector of the electron. In orbitals with an angular momentum quantum number of zero the spin-orbit interaction is zero. In organic systems three basic components carbon, oxygen and nitrogen only have the $2p$ orbital with spin-orbit interaction and thus have very weak interaction resulting in large spin-flip lengths. For this reason, organic materials are being looked at for spin transport materials in spintronic devices. The large spin-flip length means that the prominent electrons in triplet states are unlikely to recombine leading to the long carrier lifetime.

There are several proposed models for charge movement between organic molecules. The fundamental difference in the electronic structure alters the mechanism of charge transport in organic molecules with respect to the traditional band structure model. Localized states shown by the orbital structures constrain the probable movement of electrons around the molecule, thus restricting the possible locations of charge transfer between adjacent molecules. The overlap of unoccupied molecular orbitals of nearby molecules with the occupied molecular orbital of the current molecule facilitates charge transfer. Maximizing molecular orbital overlap with optimized geometries can improve charge transfer within a film. Transfer of excited electrons between molecules has been explored as either a carrier exchange process in Dexter transfer or an energy exchange in Förster transfer shown in Figure 2.3 [27, 28, 29]. Due to the large proportion of triplet state electrons, understanding transfer mechanisms governing movement of electrons in molecular systems is needed.

The mechanism for carrier transfer between molecules is still uncertain, there are three models to consider: Percolation, Poole-Frenkel, and Band theory [30]. Percolation theory, also known as hopping theory, views the occupied molecular orbitals and unoccupied molecular orbitals as a combination of localized states. Electrons then occupy and hop between these states via thermal and transient processes. This hopping is dependent

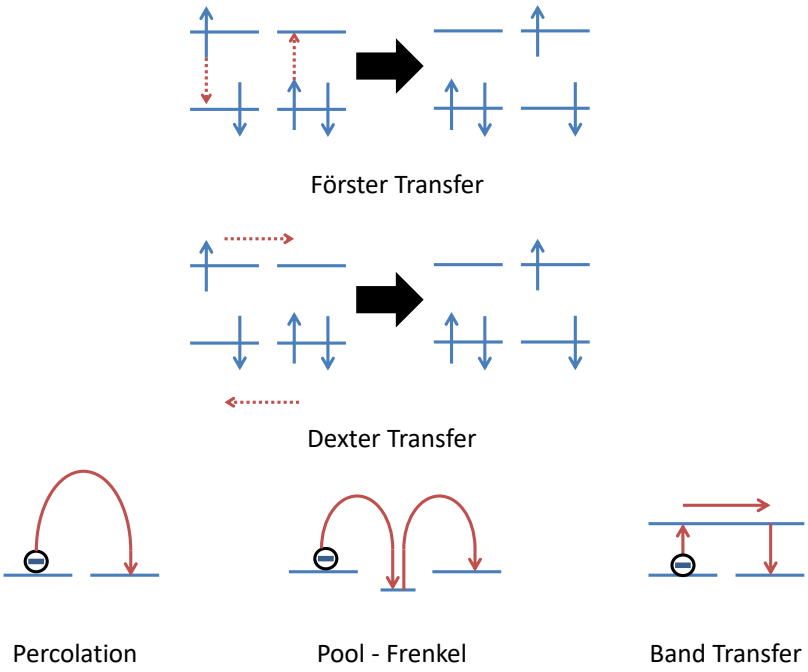

Figure 2.3: Charge transfer models and mechanisms of electron exchange in molecular systems.

on the transition between localized states, limiting to probability of charge transfer. Poole-Frenkel theory uses bands and introduces localized trap states. Trapping states can aid or hinder conduction depending on the probability of charges to enter and exit the trapped state. In the Poole-Frenkel model the localized states do not exchange charges with each other but with the conduction band. Localized states can also act as a mechanism to excite electrons from the valence band, by introducing an intermediate step. By combining hopping and Poole-Frankel a more complete hybrid theorem emerges, that accounts for both localized and delocalized nature of polycrystalline semi conducting films [30].

2.2 Working Principles and Device Fundamentals

2.2.1 Illumination

It all starts with a light source in this case the sun will be providing the desired energy to be converted to electrical energy so one must understand the emission from the sun and have a standard to use for device performance comparison. The emission from the sun can be modeled as a Planckian blackbody using Eq.

2.11 [31].

$$B_\lambda(T) = \frac{\frac{2hc^2}{\lambda^5}}{e^{\frac{hc}{\lambda kT}} - 1} \tag{2.11}$$

where B_λ is the spectral radiance of a specific wavelength λ, given the temperature T of the black body radiator. Using the effective temperature of the sun (5772 K) one can reasonably reproduce the total emission from the sun [32]. When viewed from earth however one sees only a fraction of the emission based on the solid angle which we occupy. This portion of sunlight that is incident on the earth is the extraterrestrial solar irradiance (AM 0) seen in Figure 2.4 and compared to the modeled black body radiation from a source at 5772 K [33, 34, 35].

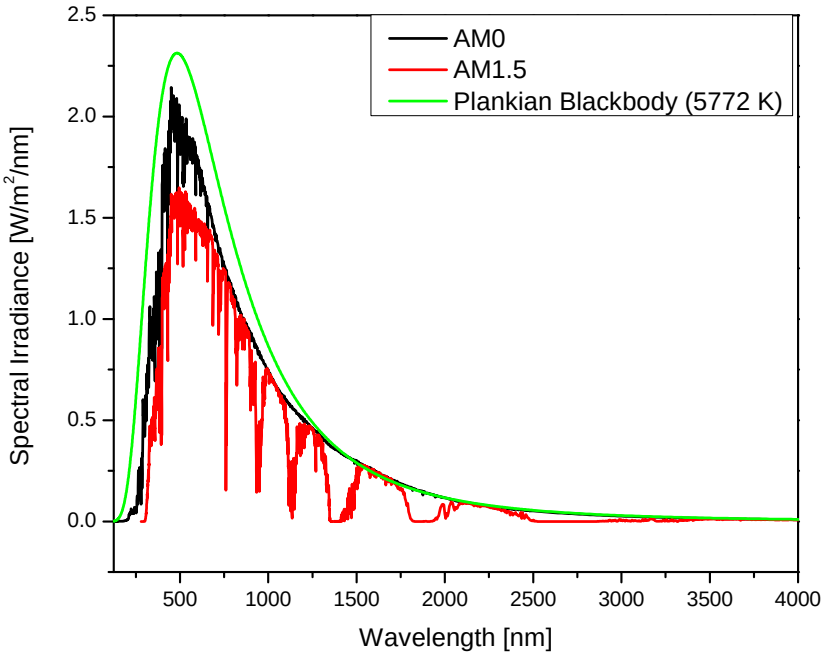

Figure 2.4: AM 0 and AM 1.5 solar spectrum standards and modeling solar radiance using a plankian blackbody radiator.

When considering solar power on earth one must consider the effect of the atmosphere on the solar spectrum. With absorption bands due to various atmospheric aerosols there is a significant change in power depending on path the light will take to the photovoltaic device. The ideal case for a solar cell on earth is to position the device on the equator pointing directly upward with the sun directly overhead, this is considered to have a filtering of one air mass (AM 1). The time of day combined with the time of year and one's latitude determine the angle at which the sun will be in the sky to a given observer. This will determine the air mass which the light must pass through and thus the change in the terrestrial observation of the solar spectra.

The Simple Model of Radiative Transfer of Sunshine (SMARTS) software can be used to model the effect of atmospheric aerosols on the solar spectra [36, 37]. Included in the SMARTS software is an example the models the current standard in solar cell testing, Air Mass 1.5 (AM 1.5) or ASTM G 173 [38, 39]. AM 1.5 is the defined as a surface at an angle of 37^o toward the equator, with the normal vector of the surface facing the sun at an angle of 48.19^o from the normal of the earths surface as in Figure 2.5. These parameters were decided upon because they represent the average for the continental United States. The red spectra in Figure 2.4 is the AM 1.5 spectra, showing the abortion bands due to an AM 1.5 filter. The power delivered by one sun through a AM 1.5 filter is 1000 W/m^2 [40]. Concentrator solar cells use optics to focus the power of the sun onto a device there by increasing the power generated by the device, the incident power on the devices are then stated in multiples of 1000 W/m^2 or how many suns of illumination. When testing it is important to ensure the correct incident power on the device under test.

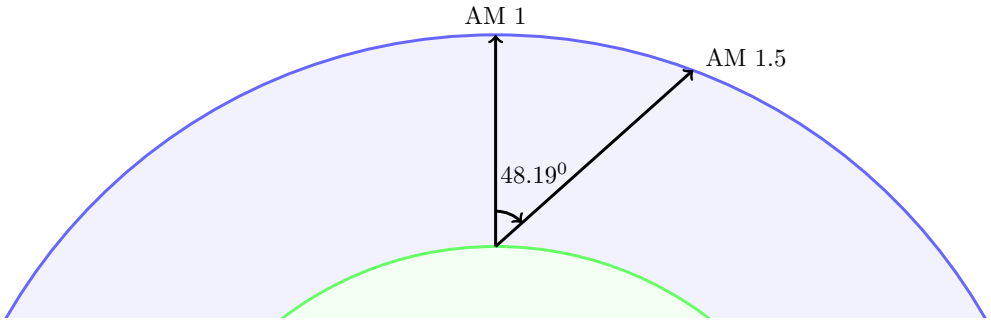

Figure 2.5: Air mass diagram

2.2.2 Device Fundamentals

Accepting Light

For a solar cell to function it must allow light into the device. To model this one can consider a device to be a series of layers, each layer is a possible point of reflection, absorption or scattering of incident light. Absorption of light is fundamental to the function of a solar device and thus will be focused on in the next section, this section focuses on the losses of light entering a device and possible methods to overcome them.

Reflection of incident light is the first cause of losses in a solar cell, reducing the amount of light that enters the device. The reflection at the interface of each layer of the device (Figure 2.6) can be modeled using Fresnel's equations of an incident wave at the interface of two materials with refractive indexes η_1 and

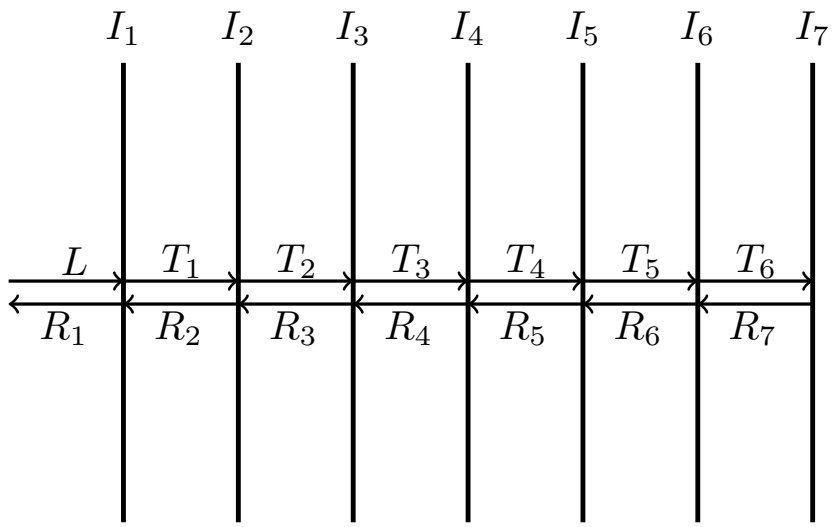

Figure 2.6: Device optical interface diagram

η_2 (Eqs. 2.12-2.15)[41].

$$\varsigma_s = \frac{\eta_1 \cos\Theta_i - \eta_2 \cos\Theta_t}{\eta_1 \cos\Theta_i + \eta_2 \cos\Theta_t} \tag{2.12}$$

$$t_s = \frac{2\eta_1 \cos\Theta_i}{\eta_1 \cos\Theta_i + \eta_2 \cos\Theta_t} \tag{2.13}$$

$$\varsigma_p = \frac{\eta_1 \cos\Theta_t - \eta_2 \cos\Theta_i}{\eta_1 \cos\Theta_t + \eta_2 \cos\Theta_i} \tag{2.14}$$

$$t_p = \frac{2\eta_1 \cos\Theta_i}{\eta_1 \cos\Theta_t + \eta_2 \cos\Theta_i} \tag{2.15}$$

where ς is field reflection coefficient separated in to perpendicular (s) and parallel (p) polarizations, Θ_i is the incident angle, and Θ_t is the transmission angle, similarly t is the field transmission coefficient. When considering the thickness of the film stack one can use the matrix formulation for thin films to more easily calculate the reflection coefficient for each layer. Calculation of transmission through several layers is done by looking at the electric ($\boldsymbol{E}^{(+)}$) and magnetic ($\boldsymbol{H}_0^{(+)}$) fields of the radiation as it passes through interfaces Eq. 2.16, using a transfer matrix $\boldsymbol{\Upsilon}$ Eq. 2.17 [41].

$$\begin{bmatrix} \boldsymbol{E}_0^{(+)} \\ \boldsymbol{H}_0^{(+)} \end{bmatrix} = \boldsymbol{\Upsilon_1 \Upsilon_2 \Upsilon_3 ... \Upsilon_N} \begin{bmatrix} \boldsymbol{E}_N^{(+)} \\ \boldsymbol{H}_N^{(+)} \end{bmatrix} \tag{2.16}$$

$$\Upsilon_{\mathbf{j}} = \begin{bmatrix} \cos\varkappa & \frac{-i\sin\varkappa}{\varpi_j} \\ -i\varpi_j sin\varkappa & \cos\varkappa \end{bmatrix} \tag{2.17}$$

Phase shift of transmitted waves is given by $\varkappa$ Eq. 2.18 using the thickness of the layer d_j. The two polarizations have differing geometric considerations thus the geometric coefficient ϖ differs as shown in Eq. 2.19 [41]. i is the imaginary unit $i = \sqrt{-1}$.

$$\varkappa_j = \frac{2\pi}{\gamma_0}\eta_j d_j \cos\theta_{tj} \tag{2.18}$$

$$\varpi_j = \begin{cases} \frac{\eta_j}{\eta_0}\cos\Theta_{tj} & , \ s\ Polarization \\ \frac{\eta_j}{\eta_0\cos\Theta_{tj}} & , \ p\ Polarization \end{cases} \tag{2.19}$$

Inputting these values into equations along with the corresponding values from the transfer matrix one can use Eq. 2.20 to determine the reflection coefficient $\mathfrak{r}$ for each film, where ϖ_i is the incident and ϖ_s is the substrate coefficient [41].

$$\mathfrak{r}_{film} = \frac{\varpi_i\cos\varkappa + \varpi_i\varpi_s\left(\frac{-i\sin\varkappa}{\varpi_j}\right) + i\varpi_j sin\varkappa - \varpi_s\cos\varkappa}{\varpi_i\cos\varkappa + \varpi_i\varpi_s\left(\frac{-i\sin\varkappa}{\varpi_j}\right) - i\varpi_j sin\varkappa + \varpi_s\cos\varkappa} \tag{2.20}$$

The reflectance on the film is then $\mathfrak{R}_{film} = |\mathfrak{r}_{film}|^2$ and the transmittance is $\mathfrak{T}_{film} = 1 - \mathfrak{R}_{film}$ [41]. Thus the amount of light that reaches the active layer can be determined and the amount reflected back through from subsequent layers. Reflected light increases the optical path length of the material but also introduces to possibility for interference. One must choose the layer thickness to avoid interference within the active layer of the device. If one incorporates an antireflective coating into the cell design, the reflection at the air substrate interface can be greatly reduced. Texture on the surface of the device can reduce reflections at angles greater than the critical angle further reducing reflections and possibly trapping light with in the device.

Several other considerations must be accounted for when one tries to maximize the light entering a device. Any contaminant on the surface of the device can lead to a decrease in the light entering the device, along the same line if front contacting materials are opaque there will be regions of the device that are shaded, this can cause issues with the device other than blocking light from entering the device by creating hot and cold spots in the device. Absorption in layers before the active layer also reduce the amount of light that enters the device to be productively converted to electrical energy.

Absorbing Light

Absorption of light is the foundation of solar cell operation. Absorption is the process by which an electron is excited from the HOMO to LUMO level taking the energy of an incident photon, creating a bound electron hole pair, an exciton. Excitons are the main consideration in a photovoltaic device, making absorption vital to device function. There are two main parameters to consider when looking at absorption of a material, the absorption coefficient, and probability of absorption.

The absorption coefficient α, shown in Eq. 2.21 is the most common parameter used to investigate absorption in materials [42]. Absorption coefficient is the factor relating decreasing intensity of light (I) passing through a material to the length of material the light is passing through with respect to the energy of the photon, given here as frequency ω. This is easily conceptualized as seen in Figure 2.7.

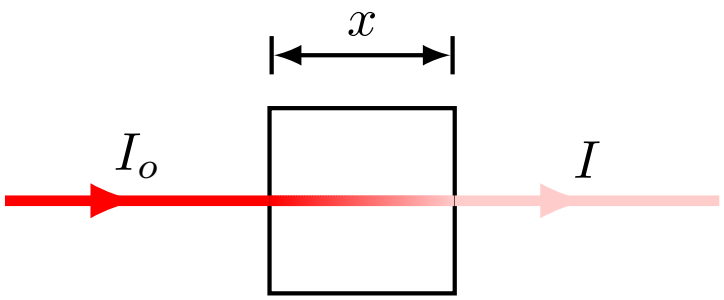

Figure 2.7: Absorption of incident light by a film.

$$dI = -I_o \alpha(\omega) dx \tag{2.21}$$

The absorption coefficient is also seen in the rate of energy absorption Eq. 2.22, combining Eqs. 2.21 and 2.22 one arrives at a form for the absorption coefficient Eq. 2.23 [42]. Where τ is time, Λ is the area through which the light is passing, $\hbar$ is Dirac's constant, and W is the transition probability of an electron in the system,

$$\frac{dE}{d\tau} = -\Lambda dI = \hbar\omega W \tag{2.22}$$

$$\alpha(\omega) = \frac{\hbar\omega W}{I\Lambda dx} \tag{2.23}$$

To better understand absorption one must look at the probability for absorption of a photon based on

the transition of an electron to an excited state, thus creating an exciton. This can be done by examining transition probability of an electron to cross the energy potential difference between energy states in the material using time dependent perturbation theory. To start one looks at the Dyson series, U_I Eq. 2.24, which is an expansion of the time evolution operator given an interaction potential V [43]. The Dyson series can be expanded to infinity by recursively substituting its self into the series. To make a useful approximation of transition probability one can make use of the perturbation expansion $c_n(t)$ given by Eq. 2.25 [43]. Where δ_{ni} is the kronecker delta function being 1 if the two indices are the same and 0 otherwise,

$$U_I(\tau, \tau_0) = 1 - \frac{i}{\hbar}\int_{\tau_0}^{\tau} V_I(\tau')U_I(\tau', \tau_0)d\tau' \tag{2.24}$$

$$c_n(\tau) =< n|U_I(\tau, \tau_0)|i >= c_n^{(0)} + c_n^{(1)} + ... = \delta_{ni} - \frac{i}{\hbar}\int_{\tau_0}^{\tau} < n|V_I(\tau')|i > d\tau' + ... \tag{2.25}$$

The total probability of transition between initial and final states provides a picture of the effect of the interaction on the entire density of states. For this one can simplify the calculation by considering the sum of probabilities for moving from state i to state n for only the first order term Eq. 2.26. The derivative of the transition probability with respect to time provides the transition rate, also known as Fermi's golden rule (Eq.2.27) [42, 43]. Where ρ is the density of states in the system,

$$\sum_n |c_n^{(1)}|^2 \rightarrow \int_{Ei}^{En} |c_n^{(1)}|^2 \rho(E_n)dE_n = \frac{2\pi}{\hbar}|\bar{V_{ni}}|^2\rho(E_n)t|_{E_n=E_i} \tag{2.26}$$

$$w_{i\rightarrow n} = \frac{2\pi}{\hbar}|\bar{V_{ni}}|^2\rho(E_n)_{E_n=E_i} = \frac{2\pi}{\hbar}|\bar{V_{ni}}|^2\delta(E_n - E_i) \tag{2.27}$$

With a semiclassical view the Hamiltonian of the electron exposed to an electromagnetic radiation can be stated as seen in equation 2.29. The electromagnetic radiation is represented by the vector potential A Eq. 2.28 [42].

$$\boldsymbol{A} = \boldsymbol{A_0} cos\,(\boldsymbol{q}\cdot\boldsymbol{r} - \omega\tau) \tag{2.28}$$

Equation 2.29 can be separated into three parts: kinetic energy, potential energy, and interaction energy. Where $\mathbf{p}$ is momentum and p is the magnitude of the momentum. The interaction component is given in Eq. 2.30, if one considers incident radiation of low intensity then the interaction can be simplified by removing the square vector potential term.

$$H = \frac{p^2}{2m_e} + \frac{e}{m_e}\boldsymbol{p}\cdot\boldsymbol{A} + \frac{e^2}{2m_e}\boldsymbol{A}^2 + V(\boldsymbol{r}) \tag{2.29}$$

$$H_{int} = \frac{e}{m_e}\boldsymbol{p}\cdot\boldsymbol{A} + \frac{e^2}{2m_e}\boldsymbol{A}^2 \;\rightarrow\; \frac{e}{m_e}\boldsymbol{p}\cdot\boldsymbol{A} \tag{2.30}$$

Substituting the interaction Hamiltonian into Fermi's golden rule Balkanski comes to a form of the absorption coefficient that clearly states the energy dependence of excitation for a two band system, Eq. 2.31 [42], where $\bar{m}_e^*$ is the reduced effective mass of the electron being examined. This can be expanded to a multi band system.

$$\alpha = \begin{cases} \frac{e^2}{2\pi\epsilon_0 c m_e^2 \omega n(\omega)} \left(\frac{\hbar\bar{m}_e^*}{\hbar^2}\right)^{3/2} p^2\sqrt{\hbar\omega - E_g} & ,\hbar\omega \geq E_g \\ 0 & ,\hbar\omega < E_g \end{cases} \tag{2.31}$$

Excitons, the result of absorption, are the bound excited electron and its hole pair in the ground state. The pairing is a result of coulomb interaction; this interaction is stronger in smaller atoms due to the reduced shielding from the nucleus by lower orbitals. Balkanski models the exciton as a hydrogen atom, this shows the binding as an energy state just below the valence energy of the system [42]. The addition of this state effectively lowers the energy gap by introducing an intermediate localized state that can be occupied, Figure 2.8. This state effectively traps the location of the excited electron however limiting the contribution to power generation.

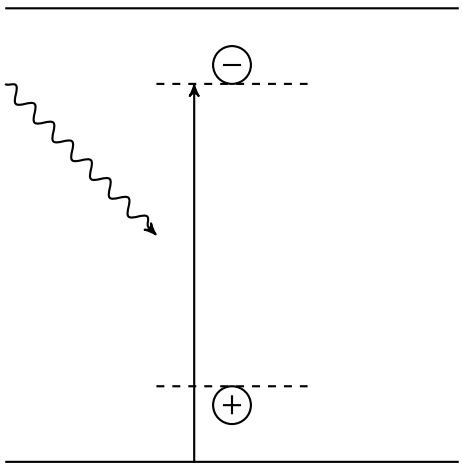

Figure 2.8: Exciton bound energy state modeled as a hydrogen atom.

Current Generation

This exciton must then be separated and have the constituent parts collected at their respective electrodes to create a photocurrent. To disassociate an exciton there must be enough energy forcing the separation of the electron hole pair. This is commonly done using a potential that is inherent in the cell, a depletion region caused by two adjacent materials with different Fermi levels. In traditional electronics this is done by making a junction between n-type and p-type materials [44]. These p-n junctions create a depletion region with a built in potential; where electrons move in one direction toward the n-type, and holes move toward the p-type side of the junction as seen in Figure 2.9 [45].

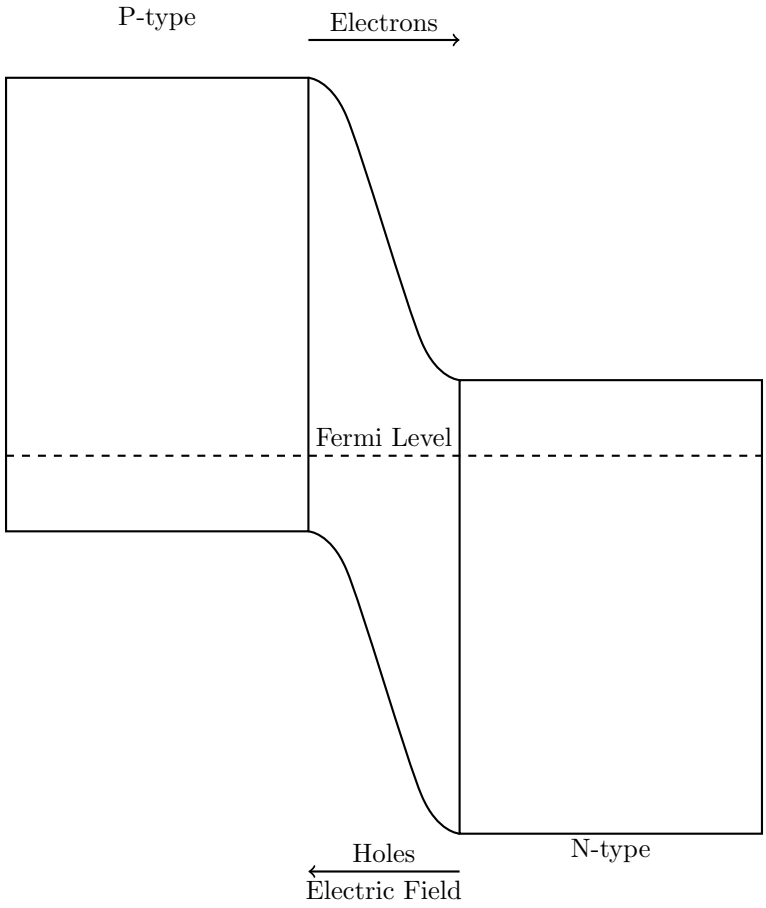

Figure 2.9: p-n junction showing depletion region and electric field produced.

Organic photovoltaics use a similar approach but employ organic materials as the active material. The HOMO and LUMO levels form an energy gap in the molecules and/or polymers of the active material and the strongly bound exciton formed from the absorption of an incident photon of appropriate energy is bound within this energy gap in a localized trap until it is dissociated [1]. Disassociation typically occurs at interfaces

within organic devices. By placing two molecules close to each other with different HOMO and LUMO levels, considered a donor and the other an acceptor of electrons, one can create an electric field to dissociated the exciton. Additionally, one can place an organic material between two metals with different Fermi levels to create an electrical potential across the organic material forcing excitons to travel within the device (Figure 2.10), encountering interfaces thus separating charge carriers. By combining the depletion regions within the device one can effectively disassociate excitons while minimizing recombination [46].

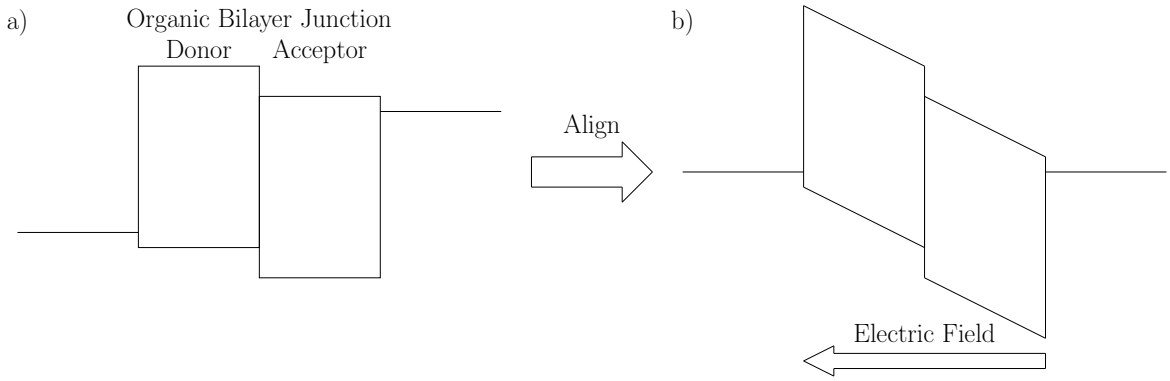

Figure 2.10: Electric field in organic devices, depicting the alignment of the Fermi energies of the two contact materials. a) Vacuum energy aligned system b) Fermi energy alignment of contacts with constant electric field throughout organic material

2.2.3 Device Structures

Active Layer Architectures

There are three basic structures for an organic photovoltaic device (Figure 2.11), a single material active layer, a multilayer planar structure, and a multimaterial-mixed structure or bulk heterojunction (BHJ). There are several reasons why one may choose one structure over another including ease of fabrication, exciton disassociation and effective absorption [1, 45, 46].

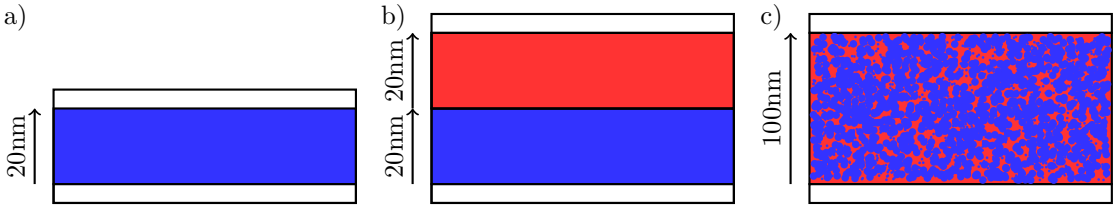

Figure 2.11: Device architectures a) single material planar structure, b) two material planar structure, c) two material bulk heterojunction.

An exciton has a limited carrier life time, the disassociate before it will combine, this is related to the

diffusion length of excitons in organic materials. The diffusion length is the average length an electron can travel before interacting within the material, for organic materials this tends to be on the order of 10 nm [46, 47]. This determines the optimal structure of the active layer in an OPV by stating the optimal phase segregation. For this reason, active layers should no have regions greater than 10 nm to an interface, for planar cells this determines the thickness of the layer thickness for the materials. In BHJ cells this means that the phases of the materials should be no larger that 10 nm. Due to the nature of the BHJ it is difficult to determine and fix the size of the material phases. This is one of the major faults in BHJ OPVs, there is work being done to fix the phases once they reach an optimal size; attempts have been done using molecules to limit the phase size. Another major point of interest is the use of polymers in such an application by using block copolymers one can have acceptors and donor groups on the same polymer chain innately structuring the active layer [48, 49]. Other attempts have been made trying to get the molecules to self assemble and more with nano-structuring.

Thermal annealing is one method by which the phases in BHJs are modified, involving the heating of the cell for a predetermined amount of time at a given temperature. Annealing should increase the order in the cell thereby increasing the size of the material phases. The nature of the organic materials causes the cells to anneal even at low temperature, during operation of the cell [50]. This leads to an efficiency curve for BHJ OPVs which peaks initially as the phases are optimized and falls off over the life of the cell [51].

To improve the probability of absorption one must increase the optical depth of the cell. This can be done in three ways, increasing the thickness of the active layer [52, 53], changing the angle at which light enters the cell and reflection within the cell. Increasing the active layer thickness increases optical path of the cell in the vertical direction but also affects light traveling in directions not normal to the surface of the device. Planar cells are limited by the diffusion length of charge carriers but BHJ devices can have much greater cell thickness without running into issues with diffusion length of the excitons. The cell thickness in BHJ devices is thus limited but the series resistance of the device. If the active layer becomes too thick charge transport is impeded to a point where increasing the thickness reduces the efficiency of the device[53]. Charge transport is governed by the materials used in the active material and the method of deposition as well as solvents used.

For fabrication difficulty a single material is by far the easiest, then the bulk heterojunction and finally the multi material planar structure. The fabrication difficulty is mainly determined by the number of layers deposited. Another consideration includes solvent selection; this will be discussed further in the experimental section.

Contacts

Contacts are needed to transport charge carriers away from the photovoltaic device and connect it to a system to make use or store the energy converted. Contacts are placed on either end of the device and the materials are chosen to match the HOMO and LUMO levels appropriate for the side of the device they are positioned[1, 45]. This sets up an innate electric filed for the device aiding in the movement of charge carriers toward the appropriate contact, helping with disassociation of excitons.

Light must enter the cell through at least one face of the device, thus in traditional solar cells the front contact consists of silver finger like electrodes, the spacing on these electrodes takes into account the recombination of charge inside the active material[45]. Smaller fingers are used that then join a larger conductive branch and finally the contact point for the device. The use of opaque contacts leads to shadowing of a portion of the device lowering the efficiency and creating discontinuity in the electrical characteristics, which can lead to hot spots in the device and eventually lower the device life time. Some cells use transparent contacts for a portion of the contact to reduce the need for branching of the opaque electrode effectively increasing the diffusion length of the charge carriers, and reducing the effect of shadowing on the cell [54, 55]. There is an additional choice for the back contact, if one wishes they may fabricate a device that allows a portion of the incident light to pass through. Other options include opaque non reflective and reflective contact materials. Typically, reflective materials are used to increase the optical depth of the devices.

Ultimately the contact material must effectively move charge carriers to and from the device. The resistance of the material must be sufficiently low, not significantly limiting the current produced by the device. The contact material on the substrate must be sufficiently smooth to facilitate device fabrication without introducing failure due to electrical shorts [56]. Buffer layers are essential to facilitate charge transport to and from active materials and the contacts.

Buffer Layers

Buffer layers serve multiple purposes charge blocking, charge transport, optical buffer, and physical buffer [57]. The appropriate choice of buffer layer can greatly change the function of devices in some cases reversing the flow of charge carriers [58]. Another choice of buffer layer may improve device yield. A single buffer material can fulfill multiple functions.

Charge blocking buffers are used in organic devices to improve efficiency, by reducing the number of excitons that are quenched at an active material and contact interfaces[1]. Transport layers function by matching the HOMO or LUMO levels of the active material and reducing the energy difference between the active layer and the respective contact one can improve the conduction in the device. Many of the charge

blocking materials are also transport materials improving a specific charge carrier movement between layers, while at the same time increasing the energy required for transport for the other charge carrier [59]. In some cases, multiple buffer layers will be combined to achieve this effect, this increase device complexity but also can improve device efficiency. This is a late stage optimization step as detailed information about the active material is required to make the appropriate choice of buffers. One can effectively dictate the direction of charge movement by selecting the appropriate charge blocking and transport materials.

All buffer layers must have their optical properties scrutinized within a photovoltaic device. The buffers at the front of the device must allow as much light to enter the device and can be used to reduce reflections at the interface between the front contact and the active material. To do this the thickness of the buffer must be finely controlled and the refractive index of the material must also be considered. Optical buffer layers of transparent conducting materials can be used to provide an appropriate space to reduce the effect of destructive interference in cells that employ reflection to trap light within the device [53].

Physical buffer layers are used for a variety of reasons but are fundamentally used as a sacrificial layer that will improve conduction while reducing the interaction between the contact and the active material. In cells that employ indium tin oxide (ITO), a material with a larger root mean squared roughness, as a front contact a physical buffer layer is used to smooth the surface of ITO to reduce shorts in the device [57]. Metal deposition on top of organic material will likely damage the organic film. Metals have a much higher deposition temperature than organics and can sputter organic molecules off of the surface on which they are deposited. Metals can also diffuse into the organic films creating quenching centers and possible shorts with in the device [60]. Reducing the interaction with the metal and the active material can greatly improve the efficiency of the cell. Employing a physical buffer that will not be greatly affected by the metal and can block recombination at the metal interface should improve the device function. Low temperature metal deposition such as solution processed metals can overcome this but one has to consider the solvent used and the conductivity of the metal film. Physical buffer materials are essential for device yield, by reducing variability in contact material interaction with the active material.

Modeling Device Characteristics

Photovoltaic devices can be modeled by a simple circuit, shown in Figure 2.12 [1, 45, 61]. Where $\mathcal{I}$ denotes current and $\mathcal{R}$ is resistance. The device is seen as a diode with an anti-parallel current source. The diode being the device operation without excitation of incident photons. In the presence of solar radiation, the current source provides the photo current generated. Defects in the device lead to a shunt resistance and the conductivity of the device determines the series resistance.

A device can be modeled using Eq. 2.32[61] and roughly approximated as an ideal diode using Eq. 2.33

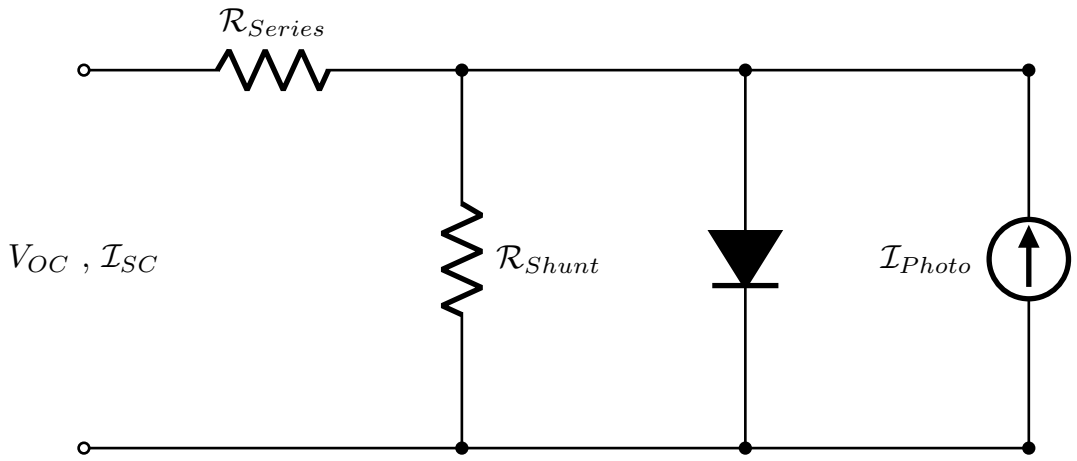

Figure 2.12: General single diode circuit model for photovoltaic devices.

[20] if the shunt resistance ($\mathcal{R}_{shunt}$) is set to a very large number, the series resistance ($\mathcal{R}_{series}$) is zero and the photocurrent is zero. Where ι is the current passing through the circuit, $\mathcal{I}_S$ is the saturation current, V is the applied potential across the circuit and V_T is the thermal voltage. For the purpose of the simulate output shown in Figure 2.13, the saturation current is neglected. The thermal voltage is given by Eq. 2.34 [20].

$$\iota = \mathcal{I}_S \left[e^{\frac{1}{nV_T}(V + \mathcal{I}\mathcal{R}_{series})} - 1 \right] + \frac{V + \mathcal{I}\mathcal{R}_{series}}{\mathcal{R}_{shunt}} - \mathcal{I}_{photo} \tag{2.32}$$

$$\iota = \mathcal{I}_S \left(e^{V/V_T} - 1 \right) \tag{2.33}$$

$$V_T = \frac{kT}{e} \approx 25mV \quad @ \quad 20^oC \tag{2.34}$$

The simulated measurement, Figure 2.13, shows two curves a dark and light curve. The dark curve is given by Eq. 2.33, and the light curve is the same but with the photocurrent subtracted. Photocurrent is subtracted from the ideal diode curve for the light current due to the testing method. Testing is done by reversing the bias on the device, then sweeping the applied potential. In this way the potential, and current produced by the device while exposed to solar irradiation can be determined. There are several parameters that can be found in a measurement plot used to quantify the function of a device and look at improvement of device design and fabrication. These include open circuit voltage, short circuit voltage, series resistance, shunt resistance, maximum power point, fill factor and power conversion efficiency [1, 45].

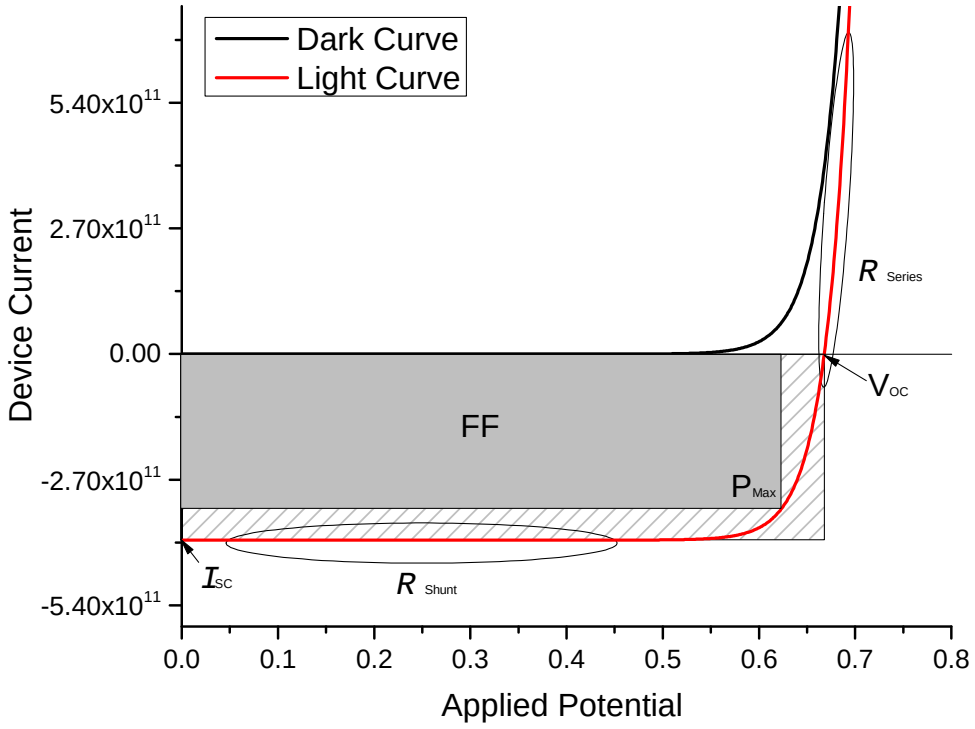

Figure 2.13: Simulated device current voltage characteristics showing the source of characteristic parameters.

The resistors in the device model greatly affect device efficiency, shunt resistance is the resistance of the first portion of the diode curve, and series resistance is the resistance in the second region. The series resistance is the dominant term once the diode turns on, limiting the current that passes through the device. Series resistance arises from the resistance of each individual layer and the contact resistance between layers. This is similar to other diode models where the diode is modeled as a diode plus resistor to account for device resistance. The shunt resistance arises from alternate pathways for charge to move through the device. These alternate pathways result in leakage current that greatly degrade the efficiency of the device. These leakage currents generally result from faults in fabrication or device design issues. It can be useful to look at the inverse of resistance, conductance when considering the properties of a device denoted by G.

Open circuit voltage (V_{OC}) is the potential produced by the device when the load is an infinite resistance, and can be found at the intercept of the light curve with the x-axis. The open circuit voltage is limited by the energy difference between the conduction band and valence band of the front and back contacts depending on the device design and the materials used. For transparent conductors the material generally has a band gap, unless a conductive polymer is used then it has an energy gap, thus in inverted devices the conduction

band, or LUMO level of the front contact will be the upper energy limit. In normal devices the valence band, or HOMO level will govern the lower energy limit. The reverse is true for the back contact, however the back contact is generally metal if a reflective back contact is used, therefore the material does not have a band gap and the limit is determined by the Fermi level of the metal. The difference between the energy limit of the front contact and the Fermi Level of the back contact contribute to the maximum potential across the device defined as the open circuit voltage [46]. This is the potential that will drive the current through the load connected to the device.

Short circuit current ($\mathcal{I}_{SC}$) is the photocurrent generated by the device when the load has zero resistance, thus is the intercept with the y-axis. This represents the total number or carriers that are available from photo excitation after the losses of the device are taken into account. Therefore, several methods can be used to increase the short circuit current from improving absorption to reducing recombination within the device as well as reducing the resistance within the device while mitigating shunt pathways. It is important to note that the short circuit current is dependent on the area of the device exposed to incident solar radiation, thus is actually a current density J. This is important when one is calculating the efficiency of the device.

The maximum power generated by a device can be found by plotting the power (P) given by the current voltage characterization (Eq. 2.35). The minimum in the plot will be the maximum power point given the negative value of photocurrent in the testing system. Using the indices of the maximum power point one can calculate the fill factor for the device.

$$P = \mathcal{I}V \tag{2.35}$$

Fill factor (FF) is a measure of how well the current device architecture is fabricated and optimized. The fill factor is given by the ratio of product of the maximum power indices to the product of the open circuit voltage and short circuit current, Eq. 2.36 [1, 45]. One can envision the fill factor as a percentage of possible power the cell is currently generating, thus given a better fabrication or optimization the device ideally could go up to 100% fill factor. This is not exactly true given the diode nature of the devices, but fill factors on the order of 80% are achievable. If the device has a linear response in the power generation region of the plot, then the fill factor will be 25% which should be the minimum fill factor for a device.

$$FF = \frac{V_{mp}\mathcal{I}_{mp}}{V_{OC}\mathcal{I}_{SC}}\text{x}100\% \tag{2.36}$$

The main factor that a consumer is interested in is the power conversion efficiency (ξ). If one were to install this device how much energy can they expect to make in a given amount of time. The power conversion efficiency is given by Eq. 2.37 [1, 45], comparing the power generated with the incident power. The efficiency

of a device is reduced by several factors, some of these factors are unavoidable depending on the device design.

$$\xi = \frac{P_{max}}{P_{inc}}\text{x}100\% = \frac{V_{OC}\mathcal{I}_{SC}FF}{P_{inc}}\text{x}100\% \tag{2.37}$$

Using these parameters devices can be characterized and by looking at the associated losses devices can be optimized.

Fundamental Losses

Several fundamental losses exist within a solar cell that limit the efficiency of a device. These can be categorized by the physical nature of the limitation (Figure 2.15): sub threshold photons, thermalization, fill factor loss, and potential drop. All of the values represented here are for single junction devices, the use of multi-junction devices can overcome some of these limitations [45, 62, 63]. All of the figures produced in this section were created using code written by Steven J. Byrnes that has been modified slightly to produce these images [64].

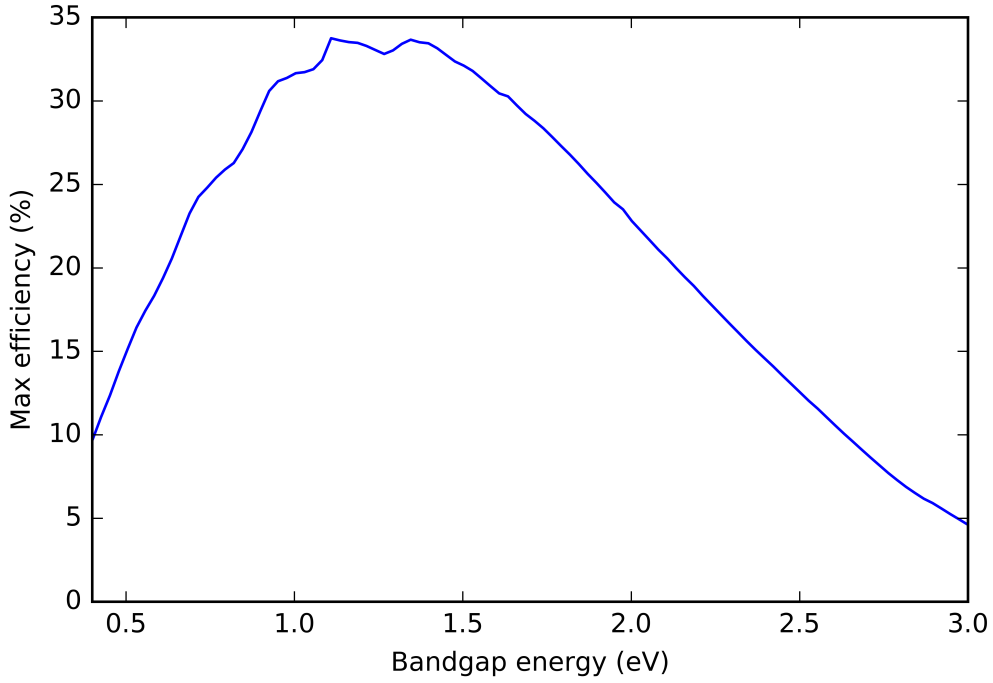

Figure 2.14: Balance limit of efficiency for a single junction solar cell with respect to band gap of absorbing material.

All of these factors can be related directly to the band gap of the absorbing materials. This was investigated by Schottky and Queisser in 1961 [62], when they determined a model to quantify the maximum

energy conversion efficiency in a photovoltaic device, called the balance limit of efficiency. The solar spectrum dictates the energy of the light that must be absorbed, and the number of photons of each energy are likely to interact with the device. A single band gap device will only optimally absorb a single wavelength of light. The optimal band gap for a single gap device shown in Figure 2.14 [64], is about 1.5 eV with a maximum efficiency of 32.1%. The main difference between the plot shown here and the one seen in the famous paper are the absorption bands in the AM 1.5 spectrum 2.4 compared to a plankian radiator which in the paper they modeled as 6000K.

The sub threshold photons are those that will be unable to excite an electron to an excited state due to a lack of energy (Figure 2.15a) [45, 63]. These are present in all devices as eliminating them would result in a large loss due to thermalization. There is an absorption mechanism utilized to overcome this and increase the potential in devices, photon up conversion. This method uses the energy of two photons that would be below the threshold energy and an intermediate state in the material to create a single exciton. For a material with a band gap of 1.5 eV the loss due to sub threshold photons is 38.5%.

Thermalization is the absorption of photons with excess energy (Figure 2.15b). The excess energy is then transformed to heat through non-radiative decay as the electron moves to lower energy states [45, 63]. Elimination of thermalization would lead to a large number of photons not being absorbed thus a balance between the two must be reached to optimize a device. Again there is a device design to mediate this loss, by using an integrated heat exchanger. The heat exchanger then converts the stay thermal energy into electrical energy, which also mitigates damage to the device caused by the increased temperature. Thermalization is attributed with 18.1% of the efficiency loss in a device with a band gap of 1.5 eV.

Fill factor loss is the difference between the ideal device and a realistic device (Figure 2.15c). An ideal device does not incorporate the resistances mentioned earlier [45, 63]. Thus the fill factor identifies the difference between the max power point and the ideal power generation, which can be seen as radiative recombination within the device. Making the minimum fill factor loss of 0.97% if the fill factor is maximized in a device with a 1.5 eV band gap absorber.

Potential drop is the difference between the band gap potential and the open circuit voltage (Figure 2.15d) [45, 63]. The band gap potential is given by the energy of the gap divided by the charge of an electron, the ratio of open circuit voltage to the band gap potential is the drop in potential. This decrease can be attributed to the difference between the energy gap of the absorbing material and the energy gap of the contact materials. There are additional limiting factors to consider including trapped states and electron transfer losses. In a device with a band gap of 1.5 eV this loss is attributed with at least a 10.4% loss.

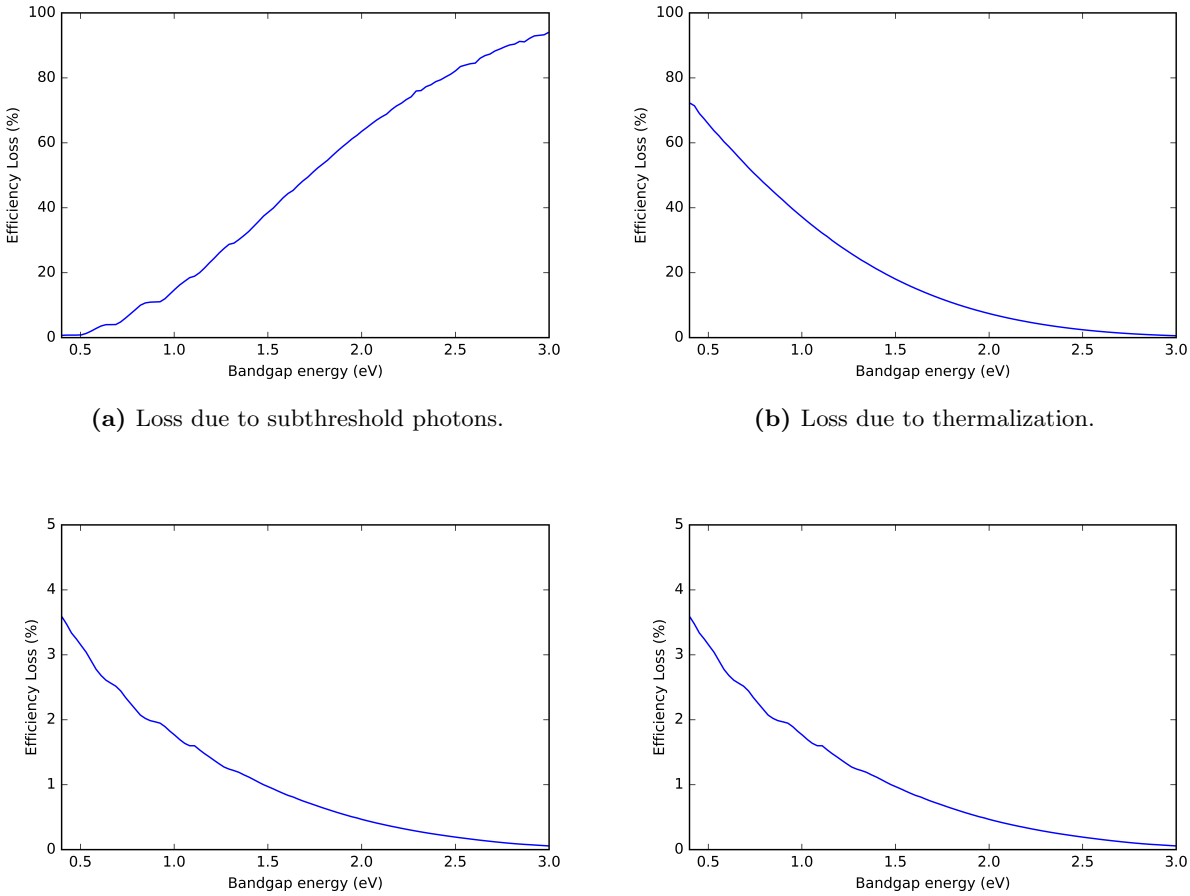

(a) Loss due to subthreshold photons.

(b) Loss due to thermalization.

(c) Loss due to fill factor.

(d) Loss due to potential drop.

Figure 2.15: Fundamental losses for a single junction solar cell. Losses due to : a)Subthreshold Photons b)Thermalization c)Fill Factor d)Potential Drop. [64]

2.2.4 Degradation of Solar Cells

Understanding the mechanisms that lead to degraded device efficiency is essential to improving device lifetimes. Device degradation can be separated into two different categories chemical and physical degradation.

Chemical degradation is the change in chemical structure of the component materials due to a variety of differing effects. One of the major concerns when considering chemical degradation is the presence of water and oxygen within the different layers [8, 65]. In the photo active layer, the ingress of oxygen an water can lead to oxidation of the polymer and small molecules. This oxidation is enhanced by the exposure to light, which provides the activation energy for reactions. Changes to the absorbing material structure can lead to diminished absorption of incident photons reducing the device efficiency. Oxidation can also lead to the formation of a quenching group such as a carbonyl, further degrading efficiency [8, 65]. Oxidation of metal electrodes can lead to increased series resistance in the device limiting short circuit current. Electrode

oxidation is more prevalent in devices that employ more reactive metals such as aluminum. Finally, buffer layers are equally susceptible to the affects of water and air. Poly(3,4-ethylenedioxythiophene) polystyrene sulfonate (PEDOT:PSS) a common buffer layer used in conjunction with indium tin oxide, transparent conductor electrode, is processed using water as a solvent. This introduces water into the core of the device thus proper care must be taken in the fabrication process. However, the acidic nature of PEDOT:PSS can degrade the indium tin oxide layer leading to the migration of indium into the device [59]. Indium ions migrating into the device become quenching locations for charge carriers greatly reducing device efficiency.

Physical degradation of device is a change in the physical configuration of the device that degrades its performance. Physical changes can be caused by a variety of external stresses, each having distinct effects on the function of the device. One major concern when fabricating a device is the external strain on the device, deformation of the device can lead to delamination of device layers and discontinuity with in individual layers of the device [8, 65]. Delamination and discontinuity can lead to open circuit like effects when testing devices, as the circuit can be severed completely depending on the level of damage. If the damage is less severe one would see a degradation in the current due to recombination at the effected area as well as increased resistance to charge flow. Another important form of physical change in organic solar cells that employ a bulk heterojunction is Oswald ripening [66]. Oswald ripening is the change in domain sizes of the two constituent materials due to thermal migration of molecules within the bulk heterojunction blend. This change tends towards a growth of the domains which alters the distance excited charge carriers must travel before reaching an interface to disassociate. If the domains grow beyond twice the charge carrier diffusion length, generally 20 nm, recombination within the device will increase substantially [51, 67]. Due to the nature of photovoltaic devices there is a considerable buildup of thermal energy due to excess energy of absorbed photons, this leads to inevitable Oswald ripening within the device.

Encapsulation is the first barrier to damage to a device, this is more important in organic devices as they are greatly affected by exposure to atmospheric conditions [65]. Encapsulation is meant to protect the device from external influences, while not impeding the function of the device. Organic material is sensitive to exposure to atmospheric conditions because it can cause oxidation of the material reducing the efficiency of device. Water can cause oxidation of the device but also delamination of the layers of the device. Ideally the encapsulation can be incorporated into the device structure, generally as the substrate on which the device is built, with the final step of attaching a back encapsulation that allows one to contact the device.

Flexibility of electronic devices requires every component of the device to be flexible as the device will only bend as much as the least flexible part [55]. Bending also introduces a unique mechanical stress that is not normally found in non flexible devices, inflexible devices must only ensure that the components are not directly exposed to extreme mechanical stress. This can be accomplished through a durable encapsulation

and mounting. Flexible devices must be encapsulated in a flexible package that allows the device to move unimpeded but still protects the device from external contamination. Organic materials are innately flexible and this holds true for organic materials used as active materials. The flexibly of organic materials come from the amorphous nature of the films allowing the molecules to move without damaging the structure of the film. Changes of the molecule due to oxidation can cause the materials to become less flexible, this holds true for many of the organic materials present in the device. Contacts must be flexible also but transparent oxides are resistant to bending and thus an alternative must be found for flexible devices, metals are innately flexible as long as they do not oxidize.

Chapter 3

Device Design and Experimental Methods

3.1 Device Design

The devices to be fabricated will have a planar structure consisting of three to five layers. The outer layers are conducting layers with optional buffer layers placed just within the conducting layers. The middle layer will be a bulk heterojunction consisting of two absorbing materials. Utilizing this basic stacking structure, a variety of materials and deposition techniques, a set of devices will be fabricated in changing atmospheric conditions. When designing a device one must consider several different aspects of the device function from basic function, and possible faults to the limitations of the current design.

Two basic device designs are investigated here, one that will have current flow toward the back contact (regular device) and one that will have current flow towards the front contact (inverted device). The initial regular device design is based on the Q1 2013 Ossila fabrication guide [68], deviations from the device fabrication were due to available equipment, the Ossila fabrication guide is updated regularly [69]. The process evolved from there as problems arose and faults were discovered.

3.1.1 Materials

There are near infinite possible combinations of materials that can be used to fabricate photovoltaic devices. The materials can be classified by the function they preform within a device. It is possible for a material to preform more than one function if used in a different device structure, in this case they will be classed by how they were used in this project. The three basic function previously described are absorption, buffer, and electrical contact. A surfactant was introduced to address a fabrication difficulty.

Organic Absorbing Materials

Absorbing materials take on many forms, here the device employs the combination of a molecule and a polymer bulk heterojunction. The molecules are based on Buckminster fullerenes, C60 the standard Bucky ball. These molecules show excellent electrical characteristics however they are not soluble; thus they have

a functionalization which degrades the electrical characteristics of the molecule but enables solution processing. Once functionalized the molecule is called [6,6]-phenyl-C61-butyric acid methyl ester (PCBM). Poly(3-hexylthiophene-2,5-diyl) (P3HT) is a polymerized thiophene that comes in a variety of molecular weights having one of two structures, rigeoregularo and regiorandom. Where the rigeoregularo tend to have a much larger conductance.

The combination of materials P3HT:PCBM in a bulk heterojunction device are very common and provide a good proving environment for changes to a cell structure. Power conversion efficiencies of these devices are not remarkably high, with the highest recorded values around 5% power conversion efficiency [57, 70, 71]. However, the P3HT:PCBM devices are proven, relatively reliable, and the starting point for this project. There are a few suitable solvents for use with this active material: chloroform, chlorobenzene and dichorobenzene to name a few. The choice of solvent is largely determined by the cosolubility of the materials, PCBM is far less soluble than P3HT. Due to the solubility of the PCBM it is advised that active layer mixtures be prepared at least twenty four hours in advance to ensure a proper mixture. This method is carried through to all other solution preparations to ensure continuity.

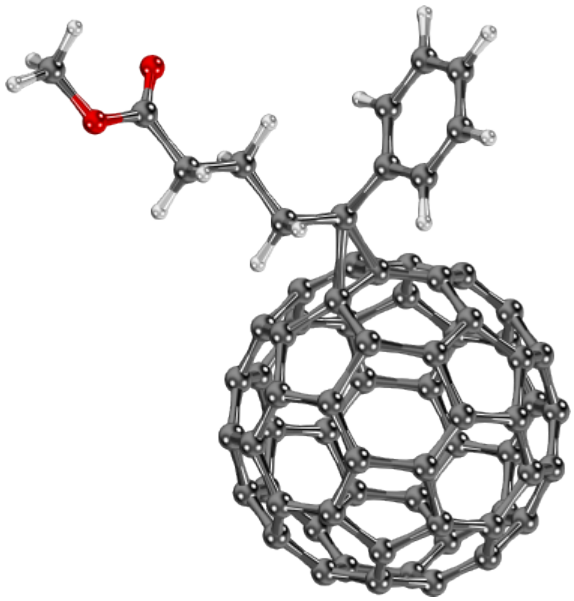

Figure 3.1: Molecular structure of PCBM

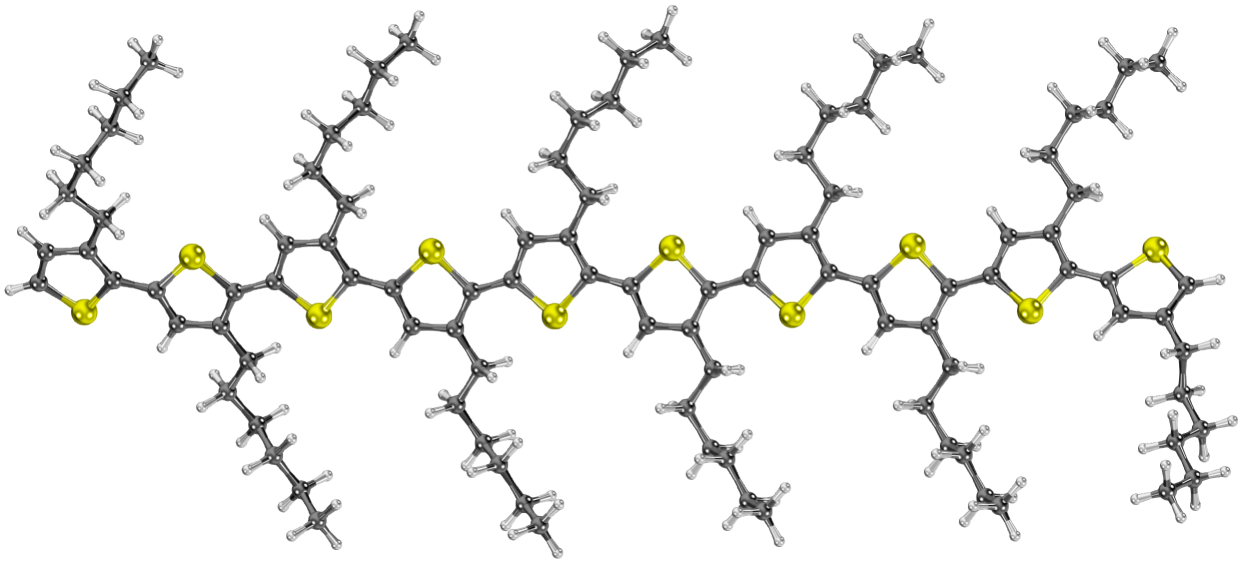

Figure 3.2: Molecular structure of P3HT

Buffer Layer Materials

Buffer materials employed for this project fit into three distinct categories: hole transport, electron transport, and electron tunnel. As such they each restrict the movement of a specific charge carrier while enabling the flow of the other charge carrier while also preforming additional tasks during the fabrication process.

PEDOT:PSS a common hole transport material having a reasonably low resistance. In some cases, PEDOT:PSS has been employed as a contact material in flexible devices. It is a very common buffer material that is often used in conjunction with the ITO to smooth the surface of the ITO to enable the deposition of subsequent layers of the device. The lowest unoccupied orbital of PEDOT:PSS is nearly at the vacuum level reducing the occupation of conduction electrons essentially blocking the flow of electrons. PEDOT:PSS is available in a few forms for this project a water dispersion is used, this introduces water into the device that is addressed in fabrication.

Poly [(9,9-bis(3'-(N,N-dimethylamino)propyl)-2,7-fluorene)-alt-2,7-(9,9dioctylfluorene)] (PFN) shares the same base structure as some promising absorbing polymers, making it a good choice for a buffer material certain devices. It also has an interesting characteristic of raising the occupation level of adjacent materials, indicating a large number of conduction stated in the lowest unoccupied molecular orbital, making it an ideal electron transport material and the highest occupied molecular orbital is sufficiently low to reduce the probability of hole transport [72]. PFN is dissolved in a mixture of methanol and acetic acid following the recommended recipe from Ossila [73].

Lithium fluoride is a common buffer layer paired with aluminum contacts due to its capability to reduce the diffusion of aluminum atoms into the active layer. Lithium fluoride functions as an electron tunnel

junction due to its high conduction band and low valence band it does not tend to enable the free migration of charge but given the thickness of the buffer layer it doe not completely inhibit the flow of electrons that have sufficient energy to tunnel through the material.

Conducting Materials

Contact materials are differentiated by their ability to function as a transparent contact. Metals can be deposited thin enough to be used as semi-transparent contacts however for this project indium tin oxide will be used as a conductive oxide material. Indium tin oxide is a favorite for use in optical device applications due to its large transmission range which encompasses the entire visible range, as well as it low resistance. There are a few issues with ITO the first being the cost, indium being a rare material and the increased demand due to the increase in electronic displays, has driven the price up. Additionally, the nature of conductive oxides means that ITO is brittle and prone to fracturing under strain, this can be reduced by fabricating thin ITO layers however the conductivity of the material suffers as the thickness is reduced. ITO tends to have a rough surface making devices fabricate without proper care prone to pinning, where there is a short from the front contact to the back due to a rough portion of the contact. ITO is processed using spray pyrolysis which is a heated combination of two or more precursor materials on a surface typically to form an insoluble film. Substrates were purchased that were quartz glass coated with ITO. Two different substrates were utilized; initially microscope slides coated with ITO were purchased from Sigma Aldrich then patterned substrates were purchased from Ossila [74]. For the back contact where transparency is not required and reflectivity is an advantage metals will be used. The metal employed will be determined by the energy level matching required for the device. Two metals are employed, gold and aluminum the Fermi levels of these metals can be found in Table 3.1 [70, 75].

	P3HT	PCBM	PEDOT:PSS	PFN	LiF	ITO	Al	Au
HOMO / VB (eV)	-5.0	-6.0	-5.1	-5.6	-1	-5.1		
LUMO / CB (eV)	-3.0	-3.8		-2.1	-14			
Work Function (eV)							-4.3	-5.1

Table 3.1: Material energy levels with respect to vacuum level, for device design. [70,75]

Surfactant

Surfactants are used to reduce the surface tension between two liquids or a liquid and a solid. In this project common dish soap is used to enable the coating of PEDOT:PSS onto a P3HT:PCBM active layer when inverting the device structure. Due to the different solvents required for the various materials there is an energy mismatch that does not allow PEDOT:PSS to coat a layer of P3HT:PCMB. The contact angle at the

interface between the PEDOT:PSS droplet and the P3HT:PCBM layer was greater than 90^o such that the drop seemed to stand on the layer. Addition of soap seemed to remove the surface tension entirely and the drop flattened out over the surface. This idea was proposed by Dr. John Purdy, the father of Dr. Sarah Purdy a former colleague.

3.2 Fabrication methods

There are two types of fabrications method employed for this project solution and physical deposition. Solution deposition method require that the material to be deposited is solution soluble. Solution processing methods tend to be much less expensive than a physical alternative. All solution processing for this project was preformed using spin coating. A single physical deposition method is available for this project, physical vapor deposition. The main requirement of physical vapor deposition is that the material is stable under extreme heating or that it will vaporize before breaking down.

3.2.1 Spin coating

Spin coating essentially evenly spreads a fluid over a surface to deposit a material in a uniform repeatable manner using minimal material. The key is to shear the fluid to disperse it evenly over the surface, to accomplish this the sample is spun at an appropriately high rate. The solution is dropped onto the spinning substrate and coats the surface with the thickness and continuity of the coating depending on several parameters including: surface energy, and cleanliness, solvent volatility, and viscosity, and finally spin speed.

Figure 3.3: Spin coater

Defects in spin coating

The most common defects that are easily identified in spin coating are particulate on the surface, insufficient solution, to slow a spin speed, and mismatched surface energy [76]. Particulate on the surface will generally appear as streaks in the deposited film that resemble comets with a curve at the start and a tail. Particulates are directly linked to a failure to clean or an extended exposure to atmosphere between film depositions. The effect of the particulate is that the film is discontinuous thus will likely cause devices that include the discontinuity in them to fail. This reduces the yield of a fabrication depending on the density of particulate and the location of the particulate. To reduce the probability of particulate fabrication must be done quickly reducing the time between cleaning and encapsulation to improve the possibility of devices working properly. When one does not drop enough solution on the substrate the solution will not completely wet the substrate surface. Not completely wetting the substrate will have different effects depending on the layer being deposited, but cells that are not entirely coated are likely to fail and will have a lower efficiency. One can solve this in a few ways the simplest is to use more solution. If one does not wish to use more solution then one could change the solvent to one less volatile, or change the viscosity of the solution by reducing the solute concentration. A solution that may be overlooked is the temperature of the substrate, if the deposition follows a baking step then one should consider waiting for the device to cool before depositing the subsequent layer. Reducing the temperature of the substrate will reduce the rate at which the solvent evaporates increasing the wetting of the substrate. If the spin speed of the substrate is to slow then the solution will not shear leaving the substrate wet after spinning this leads to an uneven coating and may not fully coat the substrate. The result of regions that are too thick will be that the resistance in those regions is larger than in others leading to a non uniform current density in the device. Overcoming a low spin speed is simple by increasing the rate the substrate is spinning one should be able to find a speed at which to deposit the thickness of film they require. If the speed at which the solution shears is too high to make a film sufficiently thick one can increase the concentration of the solution. Surface energy mismatch is seen when the solution does not coat the substrate but is ejected from the surface during deposition. Resulting in the absence of the desired film changing the characteristics of the device. Surface energy mismatch is much more difficult to overcome than previous coating problems, either the solution or the substrate surface must be altered, while maintaining the electrical characteristics of the design [77]. Cleaning processes can be used to treat the surface of the substrate altering the surface energy, these usually involve changing the oxidation of the surface which can adversely affect the conductivity of materials such as graphene. One can change the solvent that has an appropriate surface energy, this will likely change the solubility of the solute in the solvent. An alternative to changing the solvent completely is to used a mixed solvent to alter the surface

energy this takes time and experience to choose appropriate additives.

Surface energy affects how well the solution will wet the substrate surface, this is along the same line as the mixing of water and oil. If the energy is mismatched the solution will not coat the substrate but fly off the surface. There are several techniques that can be employed to alter the surface energy of a substrate or solution, like adding soap to water to mix with oil. A method to test if the solution and the substrate surface energies are compatible is to place a droplet of the solution on the substrate and observe the angle of the solution where it intersects the surface of the substrate, this is the critical angle [77]. If the critical angle approaches 180 degrees it is well matched and will coat the substrate well. Critical angles closer to 90 degrees or less mean the surface energies of the solution and substrate are not well suited for deposition.

Cleaning is the removal of contamination from the substrate. Types of contamination vary and the method of removal also varies. To remove organic contamination one can use organic solvents such as acetone, ethanol, and iso-propyl alcohol. Other methods are also used to remove organic material, basic solutions such as sodium hydroxide or UV radiation to etch away the organic material, these two methods can also be used to make the substrate surface hydrophilic changing its surface energy. To remove oxide layers hydrofluoric acid can be used. It is important to note that cleaning is important for a variety of reasons depending on the nature of fabrication and the type of contamination considered.

3.2.2 Physical vapor deposition

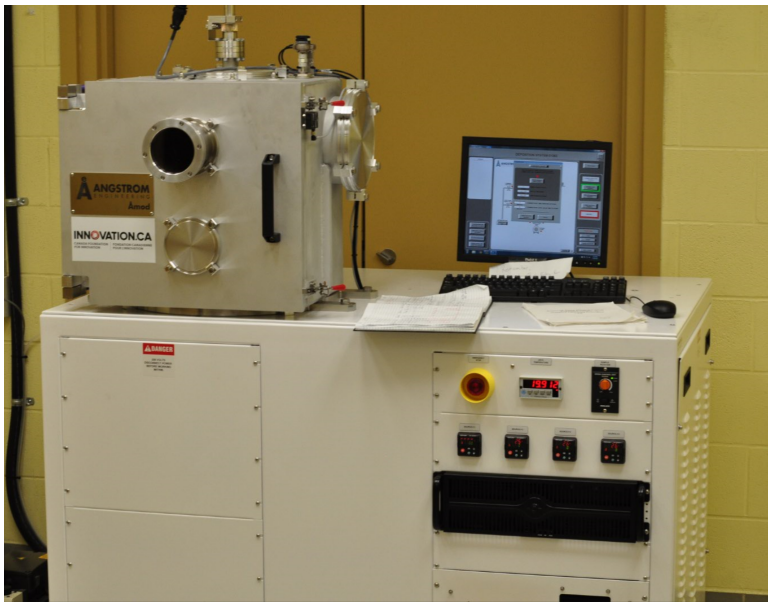

Figure 3.4: Physical vapor deposition system

Physical vapor deposition is the process of evaporating or sublimating a material then depositing the on

a substrate positioned above the vaporizing material in a chamber under high vacuum. Deposition using this method is highly controlled using a crystal oscillator to measure the deposition rate and thickness, using the feedback from the crystal oscillator a proportional integral derivative controller maintains a stable deposition rate.

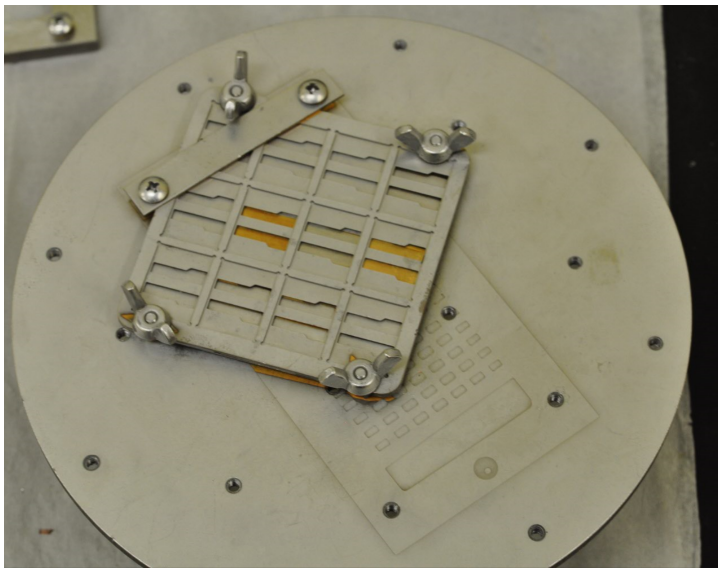

Figure 3.5: Ossila shadow mask for patterned substrates.

Masking of the sample allows for more complex device structures by controlling the area of the deposition. The deposition vapor rises from the sources in the evacuated (10^{-8} Torr) chamber in a cone, to evenly coat the samples the sample plate rotates at a slow speed to minimize shadowing due to rotation of the sample plate. Physical vapor deposition enables the deposition of a variety of materials with the main consideration to if the sample will be altered during the deposition process. Materials can be placed in one of two different sources one is a resistive heater, or a furnace for deposition. The system used was an Angstrom Engineering Amod PVD which had a single resistive heater and four furnaces. The multiple sources allow one to deposit two materials at the same time, or a series of depositions without breaking the vacuum. Resistive heaters are generally used for materials that are resistant to change during rapid temperature changes, where furnaces use crucibles which dampen the change in temperature making them ideal for sensitive materials, and lower temperature depositions due to the precise temperature control. The resistive heater has a wide variety of element options, depending on the material being deposited and the desired rate of deposition. Aluminum for instance wets, and alloys with the boat, tungsten the material most common in resistive heater boats; to avoid this one can use an alumina coated boat to resist alloying or wire basket to maximize surface area to prevent aluminum from coating the resistive heater mounting points. One must also consider the form of the material deposited to deposit aluminum it was found that switching from quarter inch diameter ingots to

eighth of an inch diameter ingots dramatically improved deposition. The furnaces have similar considerations when choosing the crucible material, it must not react with the material that is being deposited. Failure to select a proper resistive boat or crucible have different results, an incorrect boat will likely cause the deposition to fail but no further damage to the system, inappropriate crucible choice will likely not affect the first deposition but may cause the furnace unit to fail in future depositions.

Figure 3.6: Chamber interior of physical vapor deposition system.

3.3 Device Fabrication

One of the most important aspects of fabrication is cleaning. Having a clean surface to fabricate on improves contact between the layers and helps alleviate fabrication defects. Spin coating, one of the fabrication methods used, is very sensitive to surface debris. Cleaning is preformed in a few different ways depending on the substrate.

3.3.1 Cleaning Substrate

For ITO substrates the following cleaning method was followed. ITO substrates were placed in a 10 % sodium hydroxide solution and cleaned in an ultrasonic cleaner for 5 minutes. Care is taken to ensure that the ITO surface is face up in the beaker. Then the Substrate is rinsed 4 times in reverse osmosis water. This process is repeated once again to ensure the surface is clear of organic material and is hydrophilic. Just prior to deposition of the first buffer layer the substrate is removed from the final bath station and dried using

nitrogen gas. The buffer layer is then immediately deposited.

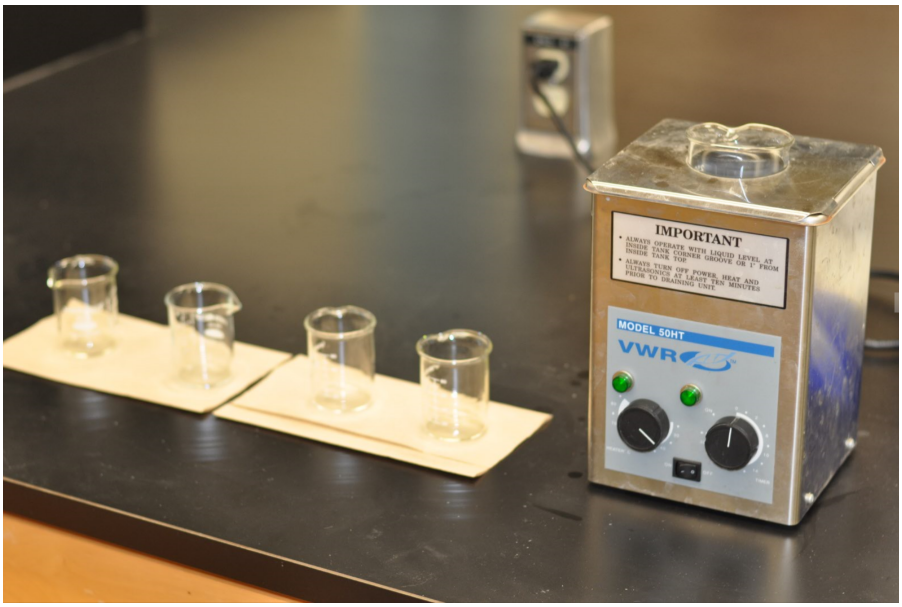

Figure 3.7: Cleaning setup with ultrasonic cleaner and four rinse baths.

3.3.2 Buffer layer deposition

PEDOT:PSS

PEDOT:PSS is purchased, from Sigma Aldrich originally the Ossila, in as a solution with water as a solvent, therefore requires a hydrophilic surface on which to deposit, in the normal structure this is not a problem the cleaning methods employed treat the surface making it hydrophilic. Inverted structures that used PEDOT:PSS however require either a different surface energy or a different solvent. After much effort it was suggested by Dr. John Purdy to use soap to modify the solvent of the PEDOT:PSS. This succeeded in making the PEDOT:PSS coat the active material, making inverted cell designs possible with the materials we have available. Prior to deposition the PEDOT:PSS is filtered using a 0.45 μm PVDF filter. The PEDOT:PSS was coated at 5000 rpm using spin coating to make the film approximately 8 nm thick, coating the surface evenly using 40 μl of solution. This coating speed works for both our inverted and normal architectures. The PEDOT:PSS is then baked at 150 ^{0}C for at least 5 minutes to remove a majority of the water from the film. The substrate is cooled for a moment after baking to ensure the temperature of the substrate does not impede coating of the active material.

PFN

PFN was purchased from Solaris Chemical as a powder that is made into a solution using a $2\mu l/ml$ acetic acid to methanol solution and is prepared to a concentration of $2mg/ml$. The solution was stirred for 24 hours prior to deposition, then filtered using a 0.45 μm PVDF filter. The PFN was coated at 4000 rpm using spin coating to make the film approximately 8 nm thick, coating the surface evenly using 40 μl of solution. This method coats the cleaned ITO surface evenly with no additional treatment.

3.3.3 Active layer deposition

P3HT was purchased from Sigma Aldrich, and PCBM from Ossila. The solution of P3HT:PCBM at a 1:1 ratio is prepared using chlorobenzene at a concentration of 25 mg/ml and mixed for 24 hours. The solution is then deposited on the front buffer layer at 2000 RPM using 40 μl of solution, yielding a film of approximately 80 nm.

3.3.4 Back Contact Deposition

Back contacts deposited onto Ossila pre-patterned ITO substrates, are masked using the Ossila shadow mask, figure 3.5. Otherwise custom masking was done for each substrate to maximize the number of possible devices, taking deposition defects into consideration.

Aluminum used as the back contact for the standard cell, lithium fluoride is an inorganic buffer layer often paired with aluminum as a back buffer layer. 10 nm of lithium fluoride is deposited using the PVD, with the furnace heating method. One must wait before the deposition of aluminum to allow the furnace to cool, stopping the deposition of lithium fluoride. 150 nm of Aluminum is deposited using $\frac{1}{8}$ of an inch diameter pellets in a resistive boat. Both lithium fluoride and aluminum are deposited using the PVD without breaking vacuum, reducing exposure to atmosphere.

Gold is the back contact for the inverted structure. Gold pellets in a resistive boat are used to deposit a 150 nm layer, using the PVD.

3.3.5 Encapsulation

Cells are sealed using a UV hardening epoxy and microscope slide cover purchased from Ossila. The encapsulation is done by placing a drop of the epoxy in the center of the cell and laying the slide cover over the epoxy, pressing down to remove excess epoxy and removing air bubbles. The cell is then placed upside down under the illumination of the solar simulator for 10 minutes to cure the epoxy. Finally, the contact legs are attached to the cell by pressing them on firmly. The cell is now ready for testing.

3.3.6 Annealing

When the active material is deposited it is likely in a highly disordered stated, and may not allow current to flow through the device in the most efficient manner. Annealing is the process of partially reordering the molecules of the active material to improve the efficiency of the cell. Annealing can be tricky as it is the main method after fabrication to optimize the cell. The morphology of the device, arrangement of molecules, is being changed from amorphous toward crystalline, to large a change and the efficiency starts to drop. As a cell ages under normal operating conditions it undergoes low temperature annealing, this degrades the efficiency of the device and contributes to the short life expectancy of organic solar cells. There are several methods that can be used to anneal a device but depending on the method it happens in different stages of fabrication. The most common is thermal annealing, where the cell is heated for a given period of time to provide energy to allow the molecules to move past each other forming larger regions of the two separate materials, this can be preformed at any point after the active material is deposited but is best after encapsulation to reduce the effect of air on the device. Larger connected regions of the same species of molecule means better charge transport in the cell. One has to keep the size of the regions in mind, too large and the excitons will recombine, causing a drop in efficiency. Another method of annealing a cell is to place it in a solvent environment, the film is allowed to restructure by releasing excess trapped solvent allowing the regions of two active materials to become more ordered and have better charge transport [78].

3.4 Device Testing

Testing was done using a OAI solar simulator with a AM 1.5 filter. The AM 1.5 filter is used to mimic light passing through the atmosphere 1.5 times due to the average angle at which light is likely to be collected, this is a global standard of photo-voltaic measurements to be published. A single sun illumination was used for testing, which is equivalent to 1000 Watts per meter squared. The cells were tested such that the external potential is in opposition to the native potential of the device.

To begin testing the solar simulator lamp is turned on and allowed to warm up for 30 minutes prior to testing, this ensures stability, and uniformity of the light source during testing. The intensity of the light source is then calibrated using the reference cell and adjusting the power until a reading of 1 sun is attained. Ideally the reference cell would be beside the device being tested to ensure stability, this is not possible with the current testing configuration. Testing is preformed by contacting the device of interest using the appropriate contacts of a Keithly 2420 source measure unit, incorrectly attaching the contacts incorrectly means the cell in forward biased and will not provide meaningful results. Then the device is positioned in

Figure 3.8: OAI solar simulator

the center of the illuminated area, and a mask is placed over the cell area to quantify the area exposed to light. The test consists of four current voltage characterization runs first with the light on and increasing the voltage and measuring the current then decreasing the voltage, this is repeated with the light off. Testing the cell in an excited and non-excited state shows the intrinsic nature of the cell, excited characteristics, and its power conversion efficiency. Changing the voltage change direction tests for inconsistencies in performance and

Testing the longevity of a device requires testing over an extended period of time under various conditions. Life cycle testing can be preformed by placing the cell under constant illumination and running periodic tests, to demonstrate changes in the cell over the time of its exposure. Utilizing these pieces of information, problems can be discovered and solutions created. Ideally these life cycle tests would be preformed in an environmentally controlled chamber, to introduce humidity, hot and cold. There are several difficulties involved in testing a solar cell, including controlling the exposed area of the device, and accounting for the change in exposure angle changing the efficiency of the device. Efficiency of devices is preformed under standard conditions as described above to create a base line for testing. There are other consumer standards

Figure 3.9: Newport reference cell

to determine durability of electronic devices such as waterproof testing, which may see use in the photovoltic industry. These will become a necessity in the organics industry as they permeate the consumer market.

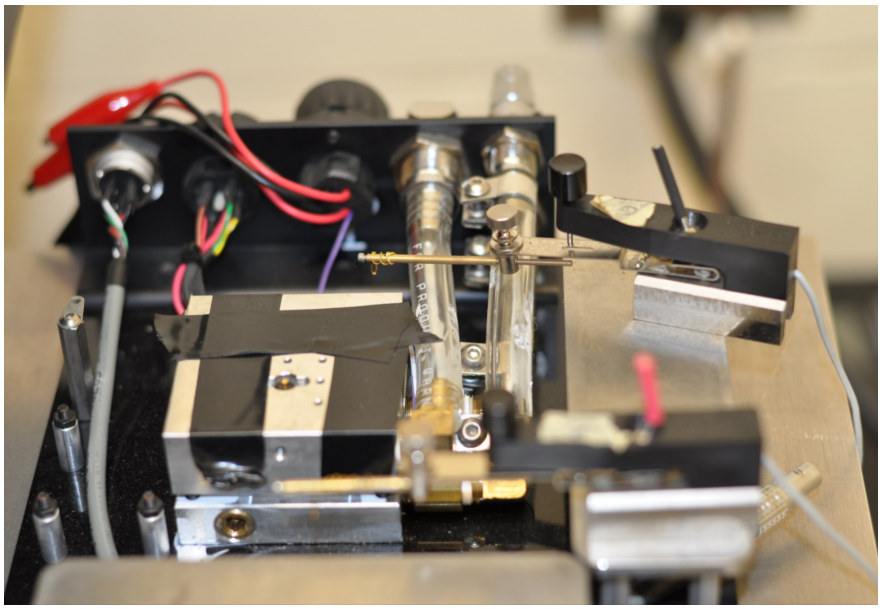

Figure 3.10: Probe station to contact custom devices.

Chapter 4

Results and Discussion

4.1 Standard Devices

4.1.1 Initial Devices

Initial devices show very low power conversion, largely attributed to the resistances in the devices and recombination effects due to faults in the fabrication method. The first device to show a photocurrent had a structure as depicted in Figure 4.1 having a current voltage characteristic shown in Figure 4.2. The PEDOT:PSS used at this point would not pass through a $0.45\mu m$ filter, likely due to high molecular weight of the material or clusters of polymer forming in solution, leading to inconsistencies in the film deposited; being the first film deposited this likely led to device failure for previous devices. The PEDOT:PSS solution was diluted in an attempt to filter the material to enhance film continuity resulting in a reduction in film thickness, this was the original PEDOT:PSS solution which was replaced later.

Cell 130220_D2

Comparing the non-illuminated and illuminated curves one can see that the device function is significantly changed when exposed to the photo excitation, Figure 4.2. The turn on potential of the device is greatly reduced and the resistance in the device seems to be also greatly reduced. The change in device function would seem to point to a fault in the device fabrication or a degenerate energy gap where the photo excited charge carriers are changing the amount of energy required to transfer into the LUMO level, by filling trapping states within the energy gap, thus are effectively reducing the potential required to pass current through the device. It is likely some combination there of because the device is meant to function like a diode, with preferential current flow in a single direction at a given turn on potential, however the line shape does not indicate the diode function intended, it is more akin to a metal insulator metal diode junction function while under illumination. A metal insulator metal diode shows a symmetric response to potential in both positive and negative values with a change in the direction of current flow. This is what can be seen in the illuminated current response to voltage. The excitation due to absorbed photons is seen in the photocurrent,

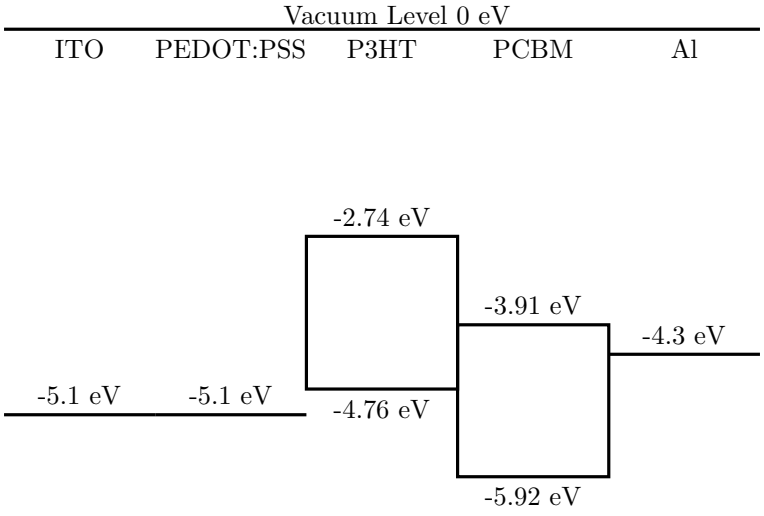

Figure 4.1: Initial device energy level diagram

act also to enhance conduction in the material well below the desired turn on potential with the photocurrent recombining quickly at a very low potential. This can be attributed to the need to dilute the PEDOT:PSS buffer reducing the electron blocking effect of the buffer layer. One possible solution is the addition of a back buffer layer to improve performance by blocking holes flowing to the back contact there by ensuring the preferential flow of charge carriers in the device.

If one considers only the characteristic values of the device as a photovoltaic device in Table: 4.1 one can see a similar story. Open circuit resistance is high indicating a large series resistance reducing the current flow in the device and the small short circuit conductance indicates a large shunt resistance thus few alternate current pathways are available. The line shape shows the region of power generation the device has an almost linear characteristic, due to the high series resistance which limits the open circuit voltage making the value extremely small. The short circuit current is small at 1.04E-05 $\frac{A}{cm^2}$ which indicates that there is incomplete absorption of incident photons. The linear nature of the power generation region leads to a fill factor that is almost as small as possible 25.9 %, because it will have a max power of half the open circuit voltage and a max power current of half the short circuit current making any device with a linear power conversion region have a fill factor of 25 %. From these characteristics one can see that improvements can be made to reduce the series resistance in the device and improve the absorption. Precedence is given to improving the intended diode nature of the device as this will allow for use of the dark curves to optimize the function of the device enabling the improvement of the series resistance and most of the other characteristics of the device.

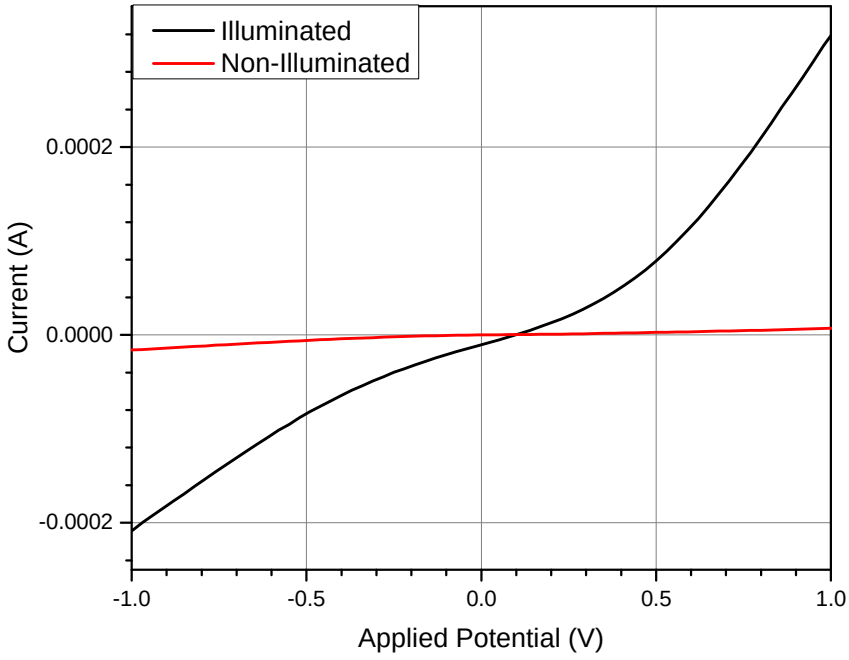

Figure 4.2: Current voltage plot of cell 130220_D2. The first cell to produce a measurable photocurrent

Cell ID	130220_D2
Voc (V)	0.097
Jsc (μA/cm^2)	-10.4
Fill Factor (%)	25.9
Roc (Ohm cm^2)	8833.7
Gsc (μS/cm^2)	155
Vmp (V)	0.0488
Jmp (μA/cm^2)	-5.37

Table 4.1: Characteristic values of cell 130220_D2

Cell 130523_D4

Improvement of the diode characteristics of the device were attained through the addition of lithium fluoride. Lithium fluoride in this structure, Figure 4.3 effectively blocks the flow of holes to the back contact reducing the probability of recombination at the back contact. By forcing the holes to flow toward the front contact the device shows the intended diode characteristics where the illuminated and non illuminated curves converge, as seen in Figure 4.4. This device shows an interesting characteristic, where the fill factor is less than 25 % but the device is still generating power Table 4.2. The negative rate of change of the curve at the beginning

of the power generation region means that the max power point consists of a current and voltage less than half of their short circuit and open circuit counter parts. Indicating the presence of an alternate non linear current pathway that is dominated by the desired diode function. If the device had a low resistance shunt pathway parallel to the desired device, then it would dominate the device function making the entire device a resistor. The displayed characteristic may be caused by a metal insulator metal diode device function seen in Figure 4.2 as the device is still very similar to the previous device but the direction of current flow has been constrained. Determination of the exact nature of the device are limited by the testing method, and lack of encapsulation, making retesting of the device improbable.

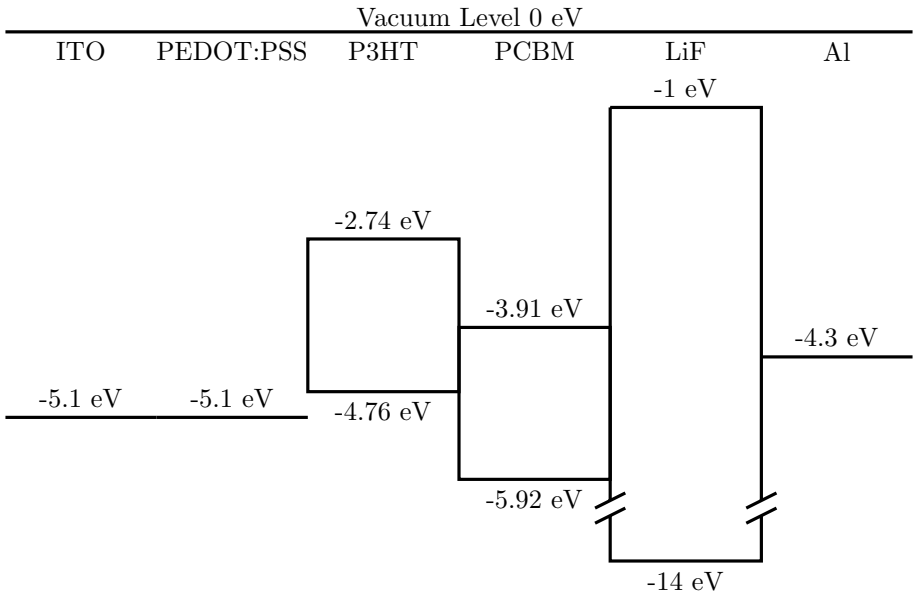

Figure 4.3: Energy level diagram depicting addition of lithium fluoride to block hole recombination

Considering the characteristic values of the device one sees a single significant improvement with the addition of lithium fluoride. There is a large increase in the open circuit voltage one would expect this result to be reflected in the other characteristic values however the short circuit current is mostly unchanged. The short circuit conductance is nearly an order of magnitude smaller pointing to a reduction in leakage currents. The open circuit resistance increased to almost five times the value seen in when compared to cell 130220_D2, considering the portion of the diode plot that is generating power the large open circuit resistance is understandable. The device is still not turned on when it crosses from generating power to consuming power. Typically, the turn on point of the diode should be the max power point of the device, pointing to a need for further refinement of the device design. The small photo current is one possible point of improvement that could limit the power generation of the devices. To improve the photocurrent one can

try several methods, such as increasing the active layer thickness however one should consider the possibility of a fundamental problem with the device.

Refinement of the fabrication process also plays a large role in the quality of the device even with the same device design. With atmospheric fabrication familiarity with the process leading to faster fabrication reduces the probability of defects in devices. As the fabrication process was streamlines and the time from cleaning to depositing the back contact is reduced the devices function improved significantly. However due to the inconsistencies in the fabrication process visible defects appear during solution processing. To improve the device yield changes to the masking procedure of the device reducing the area of the back contact to limit the effect of visible defects. This is preformed using a spin transistor mask aligned to make many devices of the best regions of the substrate. The previous masking procedure was done on a device by device basis, requiring one to cut and fit a piece of aluminum foil to the desired cell areas. This method was both time consuming and put the device at risk by requiring additional interaction with the device. By reducing the size of the back contacts and selecting carefully where to deposit the metal contact, one reduces the chance that the device area will include a visible defect. Using a mask that is rigid reduces the chance that the mask will cause damage to the device while placing and removing the mask.

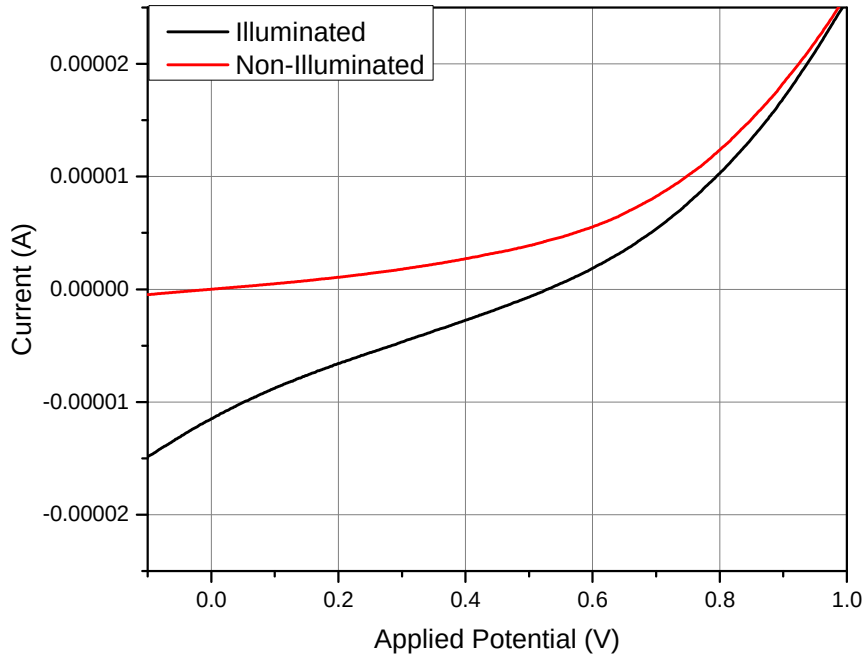

Figure 4.4: Current voltage plot of cell 130523_D4 the best custom masked standard device using lithium fluoride

Cell ID	130523_D4
Voc (V)	0.5293
Jsc (μA/cm^2)	-11.5
Fill Factor (%)	23.4
Roc (Ohm cm^2)	40661.2
Gsc (μS/cm^2)	30.4
Vmp (V)	0.271
Jmp (μA/cm^2)	-5.25

Table 4.2: Characteristic values of cell 130523_D4

Cell 140214_D1BR

Significant improvement to device function was achieved by changing the substrate from the ITO coated glass slides from Sigma Aldrich to patterned ITO slides from Ossila. The resistance of the substrates is similar with the Sigma Aldrich ITO 15-25 Ω/cm^2 and the Ossila at 20 Ω/cm^2. The thickness of the ITO layers are also very similar 60-100 nm and 100 nm respectively. Both substrates have a transmittance of greater than 78 %. The main difference in the substrates is the patterning of the Ossila substrates. By defining a cell area on the front contact one can create a region that the back contact does not vertically with overlap the front contact. The absence of an overlap enables one to contact the back of the device without the possibility of causing a short in the device or otherwise altering the device structure while operating the device. Considering the device testing system previously employed one can see that the contact for the back of the device is sharp and could cause damage to the devices while contacting. Scratches on the back of tested devices limited testing making contacting the device one of the more difficult, and unreliable, parts of the process. With the change of substrates comes the ability to encapsulate devices using an ultraviolet curing epoxy and a glass slide cover. This combination enables testing of devices over an extended period of time because the devices will not be degraded by contacting and the effect of atmospheric contaminants on the device materials is significantly reduced.

Current voltage characteristics improved in several categories, however a couple of points show a degradation. Figure 4.5 and Table 4.3 indicate the device is functioning as intended with a single non linear diode characteristic. The power generation region is now maintained past the diode turn on potential, thus the fill factor is greatly improved moving from 25% to 48%. This change indicates a significant improvement in the quality of devices fabricated, and the starting point of viable photo voltaic fabrication. The series resistance is greatly reduced with the power region including the conducting region of the diode. The open circuit voltage and shunt resistance decreased when the substrate is changed. Open circuit voltage suffers only a small reduction which could be attributed to an interface effect, as there is variation in the open circuit voltage from cell to cell. The reduction in shunt resistance is the most interesting as the illuminated

and non-illuminated device shunt resistance changes significantly. Examining the difference between the non-illuminated shunt conductance ($7.97\text{x}10^{-5}\ S/cm^2$) from the illuminated ($1.50\text{x}10^{-2}\ S/cm^2$) one can note the recombination effects in the device is significantly increased however this in proportion to the photocurrent generated by the device. Short circuit current has the largest increase of nearly two orders of magnitude over the best previous devices, indicating either an increase in photon absorption or a reduction in recombination. The fabrication process is unchanged, only the substitution of the substrate pointing towards a reduction in recombination as the active layer should maintain its thickness. A possible reason for increased absorption is the annealing effect of the ultraviolet light exposure used to cure the epoxy used to encapsulate the devices. Annealing had been avoided up to this point as the device function was not at a point where optimization would produce a great effect, however with the production of viable devices optimization has value.

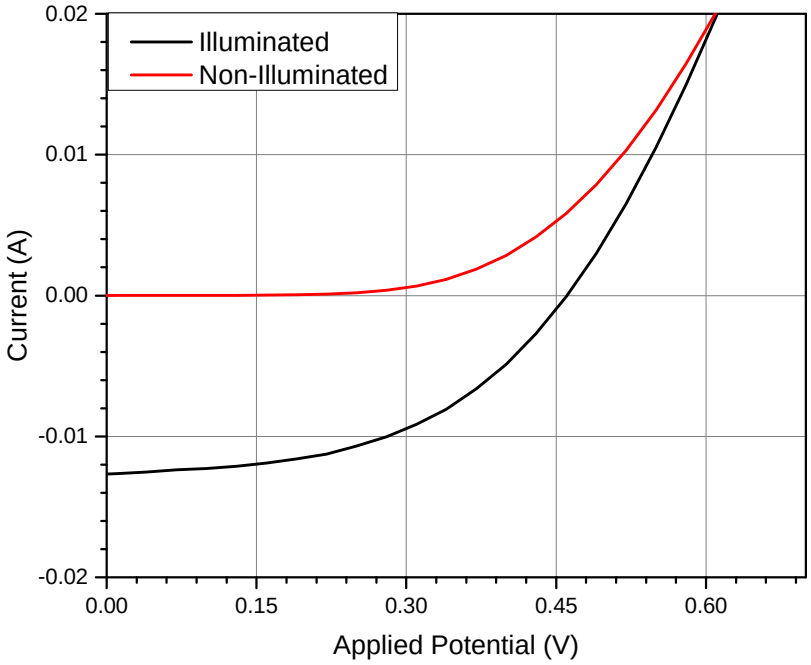

Figure 4.5: Current voltage plot of cell 140214_D1BR. The first device using Ossila patterned ITO substrate without masking the active area during testing

Cell ID	140214_D1BR
Voc (V)	0.4582
Jsc (mA/cm^2)	-12.7
Fill Factor (%)	48.8
Roc (Ohm cm^2)	11.41
Gsc (mS/cm^2)	15.0
Vmp (V)	0.3017
Jmp (mA/cm^2)	-9.38

Table 4.3: Characteristic values of cell 140214_D1BR

With devices functioning as intended the efficiency of devices can be considered. By defining the area of the device exposed to light using a mask one can calculate the efficiency of the device using Eq. 2.37 (Figure 4.6 and Table 4.4). The efficiency of cell 140214_D1BR is found to be 1.13% which is low but reasonable for a P3HT:PCBM device. Efficiency is the ultimate figure of merit in an organic photo-voltaic device, but it is determined by several factors which can be optimized to improve the efficiency of devices.

Comparing the four intrinsic values can be considered the open circuit voltage, short circuit current, short circuit conductance and shunt resistance to the unmasked device one can see a few interesting changes. Open circuit voltage of the same device has increased after masking the input area this can be attributed to the annealing effect testing the device under simulated solar irradiation will have because the non-illuminated device has also shifted slightly toward a higher turn on potential. Photo current has been reduced due to the reduction in cell area leading to a reduction in short circuit current, with the area of the device defined the short circuit current is now better represented by current density. Series resistance has increased, due to the parasitic nature of the region of the device that is now masked. The region that is now not illuminated is still part of the device but does not contribute to the photo current generation. Functioning as the non-illuminated device the region provides an addition current pathway that is less likely to conduct charge carriers until turn on potential of the device. Once turned on the non-illuminated region has a larger resistance that the illuminated region, increasing the series resistance of the device. Similarly, the shunt resistance is increased due to the combination of the illuminated and non-illuminated region shunt resistances. The fill factor is reduced to 47.5 % due to the increased series resistance caused by masking. All devices will be tested using a mask to limit the device area from this point.

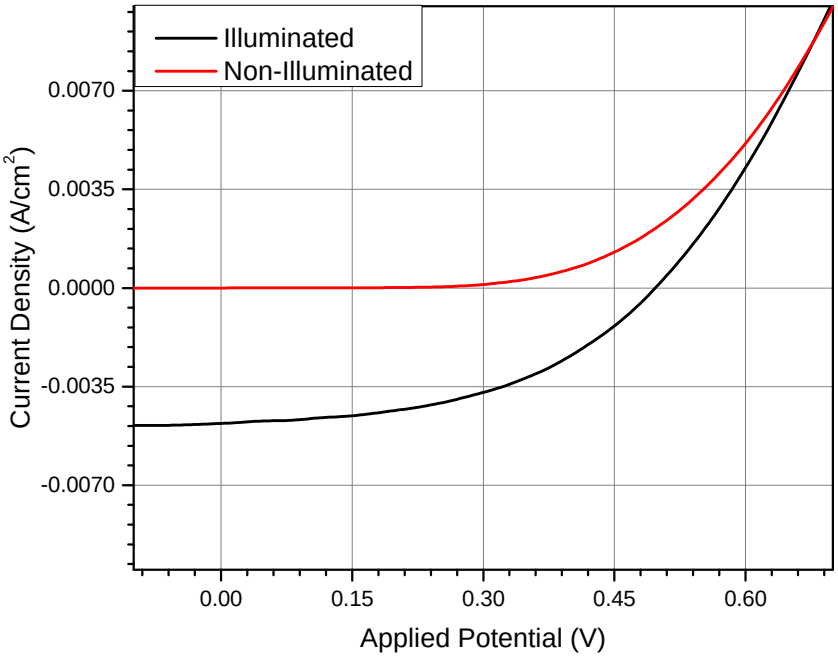

Figure 4.6: Current voltage plot of cell 140214_D1BR masked. The first run of Ossila patterned ITO substrate masking the active area during testing

Cell ID	140214_D1BR
Voc (V)	0.4942
Jsc (mA/cm^2)	-4.80
Fill Factor (%)	47.5
Roc (Ohm cm^2)	32.35
Gsc (mS/cm^2)	4.79
Vmp (V)	0.3209
Jmp (mA/cm^2)	-3.51
PCE (%)	1.13

Table 4.4: Characteristic values of cell 140214_D1BR masked

4.1.2 Optimization

Improving device design starts with improving the basic properties of the device. The first among these is the short circuit current, then come the shunt and series resistances. Improving these factors should bring an improved power conversion efficiency. These factors are connected and changes to the device will change more than one of these factors at a time, balancing the changes to optimize the performance is the key to fabricating a high efficiency solar cell.

Improving the short circuit current can be improved in many ways. Increasing the optical path of light

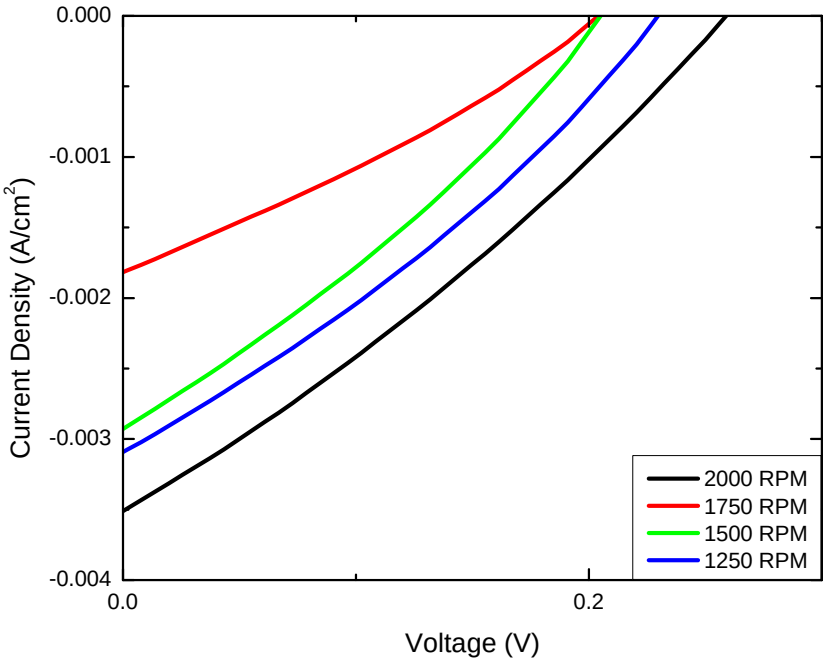

Figure 4.7: Current voltage plot depicting, effect of thickness of the active material layer, by varying the angular velocity during deposition, on device performance.

is the first way to maximize the light absorbed by the cell. The easiest way to do this is to alter the coating method to deposit a thicker active layer. One could increase the concentration of the solution which would increase the solution viscosity, increasing the thickness of the film deposited using the same spin coating parameters. An easier way to increase the thickness is to reduce the spin speed while deposition this reduces the number of solutions needed and reduces errors when comparing the devices. Figure 4.7 illustrates the average effect of increasing the thickness of the active layer, by reducing the rotation frequency from the initial 2000 RPM to 1250 RPM in 250 RPM increments. 2000 RPM is found to have the best power conversion efficiency with the largest average short circuit current and open circuit voltage. Looking at all of the curves one sees that the expected thickness does not have the expected effect the power conversion ranking. With 2000 RPM having the best function next is 1250 RPM, then 1500 RPM and 1750 RPM being the worst. If the device function was only dependent on the thickness with 2000 RPM having the largest efficiency one would expect the order to be 2000 RPM, 1750 RPM, 1500 RPM, then 1250 RPM. Fabrication of devices has a large variation in quality of devices, even with fabricating all of the devices one after the other there is a variation in the deposition of the material other than the angular velocity. The device structure is the same as that of the device seen in Figure 4.6, but the open circuit voltage of the devices tested is significantly

lower than that of the device in Figure 4.6. Pointing toward an issue with fabrication consistency, without consistent fabrication optimization is difficult. Further optimization will likely improve device performance but the nature of organic device fabrication in atmospheric conditions makes consistent fabrication nearly impossible. To attempt further improvement of devices fabricated one must look at the cleaning of the substrates and any previous materials deposited.

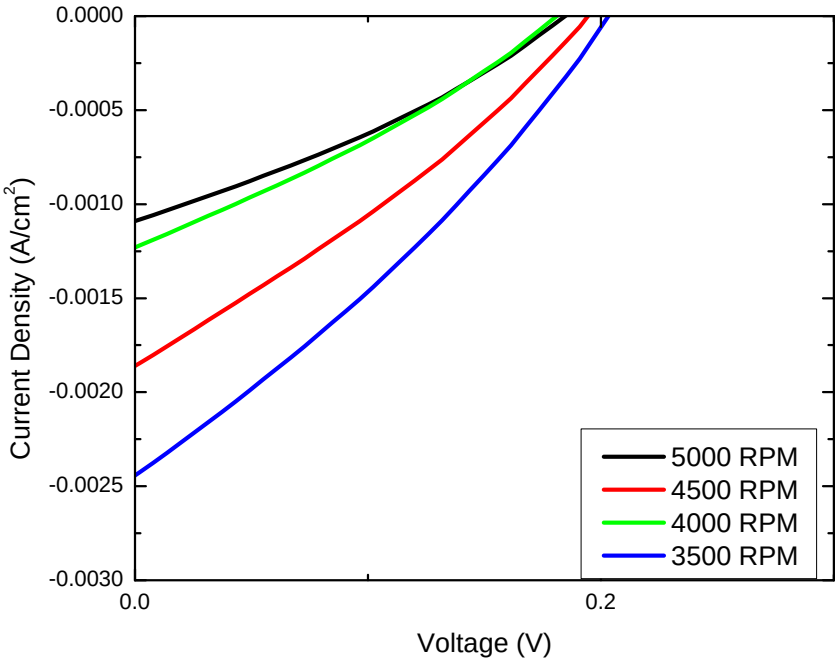

Figure 4.8: Current voltage plot depicting, effect of thickness of the front buffer layer, by varying the angular velocity during deposition, on device performance

Optimization of the front buffer layer can improve device function by limiting the recombination of charge carriers at the front contact, and improving the surface for deposition of subsequent layers. Again the easiest way to alter the properties of the front contact like the active layer is to adjust the spin speed of the spin coater. Increasing the thickness of the buffer layer reduces the probability of recombination at the front contact and the effect of the surface roughness of the front contact on the active layer deposition. Increased buffer layer thickness also increases the resistance of the device reducing the short circuit current able to pass through the device, limiting the possible efficiency of the device. Finding an optimal thickness of the buffer layer will allow further improvement of the active layer and the device efficiency should improve. The test involved incrementally reducing the angular velocity for each device by 500 RPM starting at 5000 RPM and stopping at 3500 RPM, for the PEDOT:PSS deposition (Figure 4.8). The devices fabricated are the standard

ITO substrate, PEDOT:PSS front buffer layer, P3HT:PCBM active layer, lithium fluoride back buffer layer and aluminum back contact encapsulated using UV curing epoxy and a microscope slide cover. The results show a story similar to that of the active layer optimization tests. The highest average efficiency devices were fabricated using a spin speed of 3500 RPM but there is not a clear order to determine the reason behind the increase in efficiency. If thickness increase were solely responsible then the order should be 3500 RPM, 4000 RPM, 4500 RPM, and 5000 RPM, but the results show the order to be 3500 RPM, 4500 RPM, and by a narrow margin 4000 RPM and 5000 RPM. The gap between the 3500 RPM and the 5000 RPM device show that a thicker buffer layer will likely improve device performance by reducing the amount of charge recombination this can be seen in the increase in short circuit current if the surface of the substrate were the largest gain one would expect the open circuit voltage to increase to a larger extent because there would be an greater resistance to charge movement through the device. The inconsistencies in device fabrication limit the usefulness of the results but they point toward a need to increase the thickness of the front buffer layer.

4.1.3 Best Regular devices

Changes in cell design influence various aspects of the device function by examining the effect of changing the back contact, back buffer, and front buffer layers, one can better understand device function and apply theory on practical knowledge to propose changes to devices to produce the desired effect. To this point the device design has consisted of an indium tin oxide front contact, a PEDOT:PSS front buffer layer, a P3HT:PCBM active layer, a lithium fluoride back buffer layer, and an aluminum back contact. After refining the fabrication process and attempting to improve device function by altering the active layer and front buffer layer thicknesses the best device fabricated has a power conversion efficiency of 3.23 %, Figure 4.9. The device characteristic values are shown in Table 4.5, showing marked improvements in open circuit voltage and short circuit current compared to previous devices. This device does not display the best fill factor at 44.0 % which is also shown in the series and shunt resistances. Another device that was fabricated in the same set with a fill factor of 53.2 %, however the power conversion efficiency for that device is much smaller at 0.74 %. There is significant variance between devices fabricated at the same time even between cells of the same device. These variances are due to imperfect cleaning and contamination during the fabrication process from the atmosphere. These factors contribute to inconsistencies in the solution processing of devices. The key to testing new device structures is fabricating a significant number of devices, combined with familiarity with the fabrication process to facilitate rapid fabrication the probability of producing a successful device is significantly improved. This device marks the start of a new aspect of the project where alternate device structures are tested using this device as a reference.

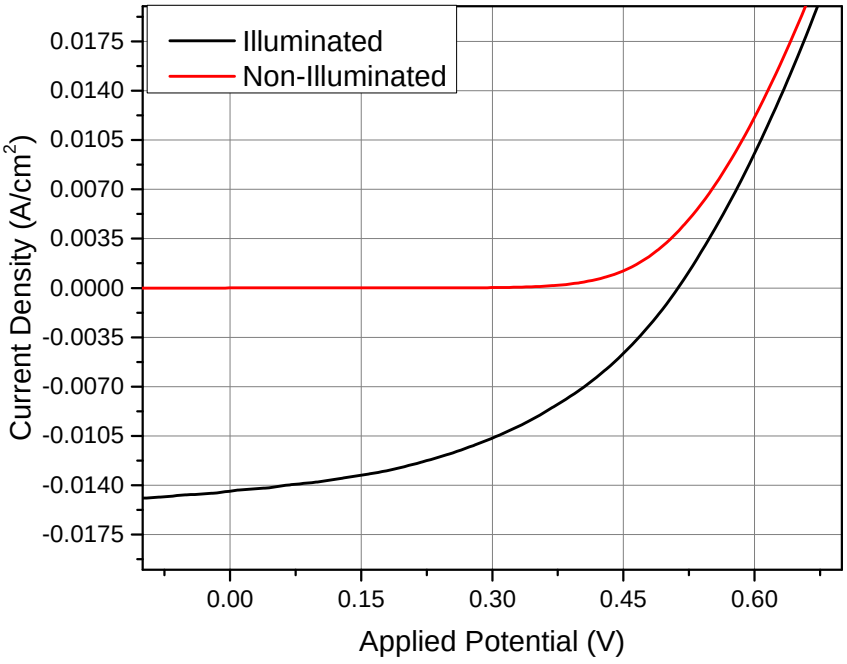

Figure 4.9: Current voltage plot of cell 140611_D2BR. Best device with the ITO/PEDOT:PSS/P3HT:PCBM/LiF/Al structure fabricated

Gold is a standard in electrical applications due to its high conductivity and relative inert nature. Aluminum is plagued with issues relating to its reactivity, interaction with the active material makes a buffer layer a necessity. The work function of gold is 5.1 eV compared to that of aluminum at 4.08 eV, when paired with indium tin oxide with a work function between 4.7 eV and 5.1 eV the potential difference between the contacts is much smaller for the gold contact [70]. The PEDOT:PSS in the structure will move the indium tin oxide toward its own work function of 5.1 eV. Figure 4.10 shows that in the current device design as the cathode gold does not align well with the PCBM LUMO level on the opposite side of the lithium fluoride tunnel barrier. The mismatch may increase the contact resistance, increasing the series resistance of the device as well as result in a significant loss of energy due when transported electrons settle into lower energy states. Examining Figure 4.11 one can see the effect of changing from an aluminum to gold contact. The open circuit voltage is significantly reduced with respect to the aluminum contacted counterpart, this is expected as the potential difference between the contact materials contributes to the innate potential of the device is dependent. Table 4.5 shows that the series resistance is increased along with the short circuit conductance while the short circuit current density is reduced. The reduction in open circuit voltage means that charges generated within the active layer experience a reduced electric field thus increasing the recombination within

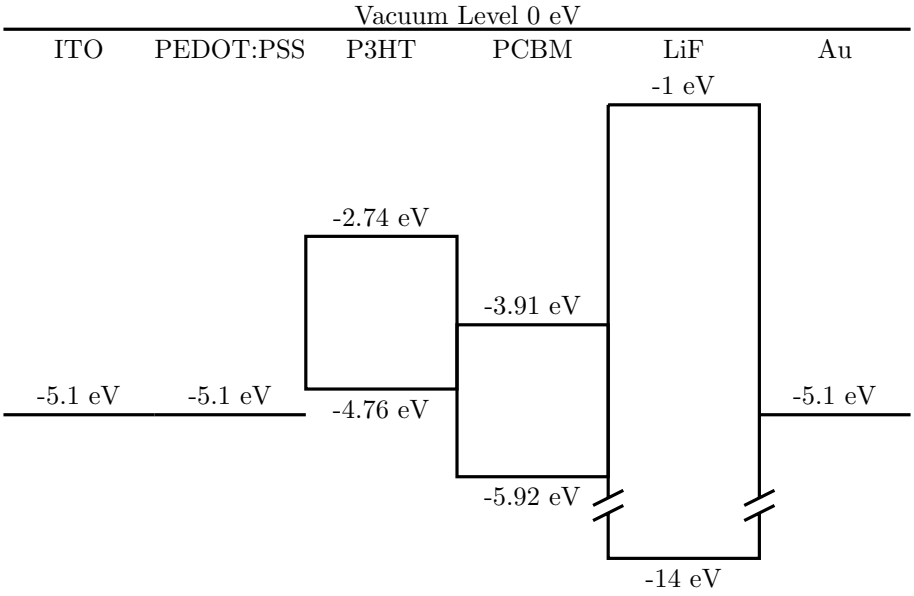

Figure 4.10: Energy level diagram showing the change in work function when aluminum is replaced with gold as the back contact

the device. An efficiency of 0.274 % reflects the detrimental effect using gold instead of aluminum as the back contact in a regular device structure. Comparing the illuminated with the non illuminated device curve one notices that the series resistance of the illuminated device is reduced increasing the current flow in the device while illuminated after the turn on the device, causing the curves to cross. After the curves cross they become parallel almost as if the turn on potential of the device is shifted by a small amount, roughly 0.015V. The reference device does not experience this effect as the illuminated and the non-illuminated curves do not cross, at a much higher applied potential the curves become very close but do not cross. This could point toward a break down of device function as seen with the very first devices fabricated however the current response curve maintains the desired device characteristics. If a front contact material with a much greater work function were employed, then the device function would be maintained and the potential within the device could be maintained.

Lithium fluoride is not an optimal electron transport material as it relies tunneling of electrons thus is mainly used to reduce the to mobility of holes. PFN is an electron conducting material that shows promise as a solution processed electron transport layer. By changing from a hole blocking tunneling barrier to an electron transport layer one may expect the photocurrent to increase, however this did not occur. Table 4.5 shows the open circuit voltage is significantly reduced, series resistance is higher, shunt resistance is smaller, but the fill factor is larger at 50.2%. The efficiency of the device is reasonable at 0.822% but smaller than the 3.23% of the reference device. The increase in the series resistance can be attributed to the increased

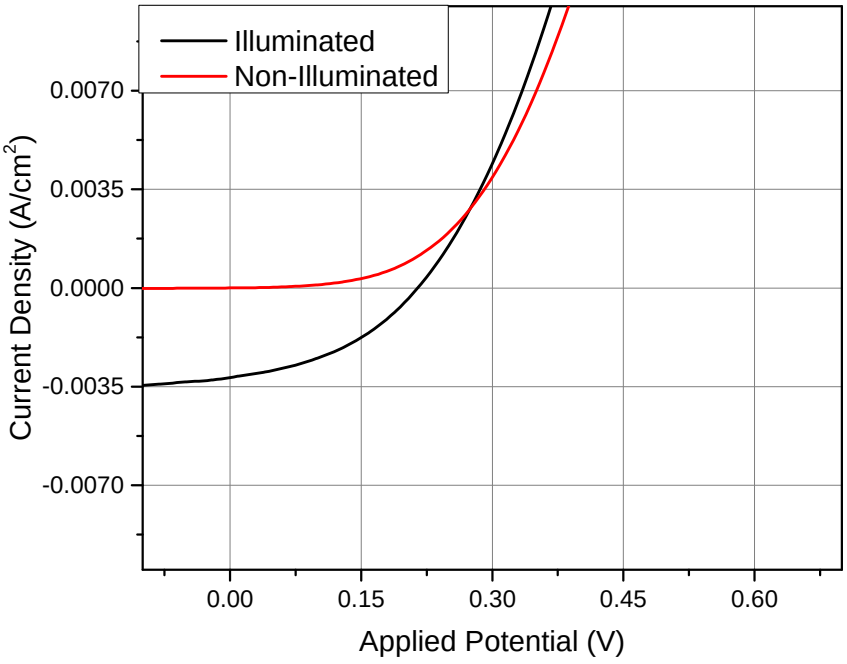

Figure 4.11: Current voltage plot of cell 140827_D4ML. Best device with the ITO/PEDOT:PSS/P3HT:PCBM/LiF/Au structure fabricated

thickness of the buffer layer as it should otherwise facilitate charge transport more effectively. Aluminum is reactive after devices with lithium fluoride were found to have a large improvement in device function it was a foundation of the device design. PFN is organic, when the aluminum is vapor deposited it is very reactive with the added thermal energy and will likely interact with the PFN buffer layer. This could have various effects increasing the contact resistance between the layers, and increasing recombination within the damaged region. The fill factor of this device indicates the resistance increase is not the most significant impact on device function as the power generation region of the device is not large enough for the resistance to have a larger impact. Thus the device efficiency loss is likely caused by recombination reducing the photocurrent and the reduced work function control due to the change in buffer layer which could also be influenced by the interaction between the aluminum and PFN. Comparing the illuminated and non-illuminated current response curves one can note a similar crossing of the curves that was noted when aluminum was replaced with gold, once again the curve become parallel after crossing. For this device however the change is more significant with a larger gap of 0.0358V forming between the curves after crossing pointing toward a larger difference in turn on potential.

Investigation of the effect of the front contact is one of the steps toward changing the device function;

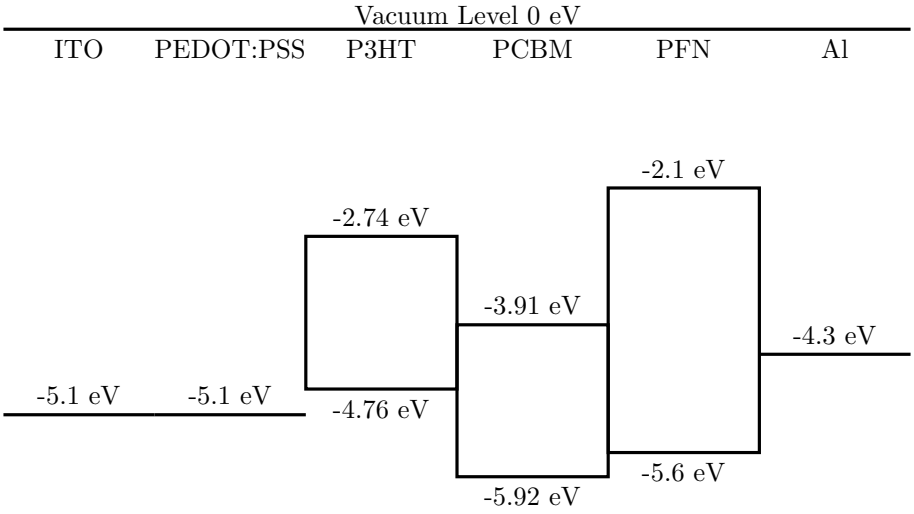

Figure 4.12: Energy level diagram for the replacement of lithium fluoride with PFN

thus testing a device where the front buffer is absent can show a few of the contributions and considerations for a replacement. The device efficiency with the PEDOT:PSS layer removed is 0.325% as seen in Table 4.5 (Figure 4.15). Resistances in the device have both degraded, the series resistance increased and the shunt resistance has decreased, combining to reduce the fill factor to 38.4%. Open circuit voltage and short circuit current are also reduced. The curves cross for this device as well although the curves do not become parallel after crossing within the measured region of the curve, indicating a difference in resistance combined with difference in turn on potential.

PEDOT:PSS was intended to smooth the indium tin oxide surface and block the movement of electrons in the conduction band of indium tin oxide to the lowest unoccupied molecular orbital of the active layer. Ossila measured their indium tin oxide as having a root mean square roughness of 1.8 nm. The PEDOT:PSS is deposited to have a thickness of between 10 and 20nm which should cover the indium tin oxide roughness. Active layer thicknesses are intended to be between 80 and 200nm, if the active layer is able to be deposited uniformly on the rough indium tin oxide surface then the variance in thickness should be negligible. Electrical shorts in the device would result in total device failure, the function of this device shows that although the smoothing aspect of the PEDOT:PSS may improve device yield it is not the essential aspect of the PEDOT:PSS function within the device.

The electron blocking hole transport aspect of the PEDOT:PSS function is therefore the more important aspect affecting the device function. Considering the energy levels of PEDOT:PSS the highest occupied molecular orbital between 5.1 and 5.2eV, which is lower than the valence band of indium tin oxide. Holes flow from the PEDOT:PSS toward the indium tin oxide likewise the active materials have lower highest

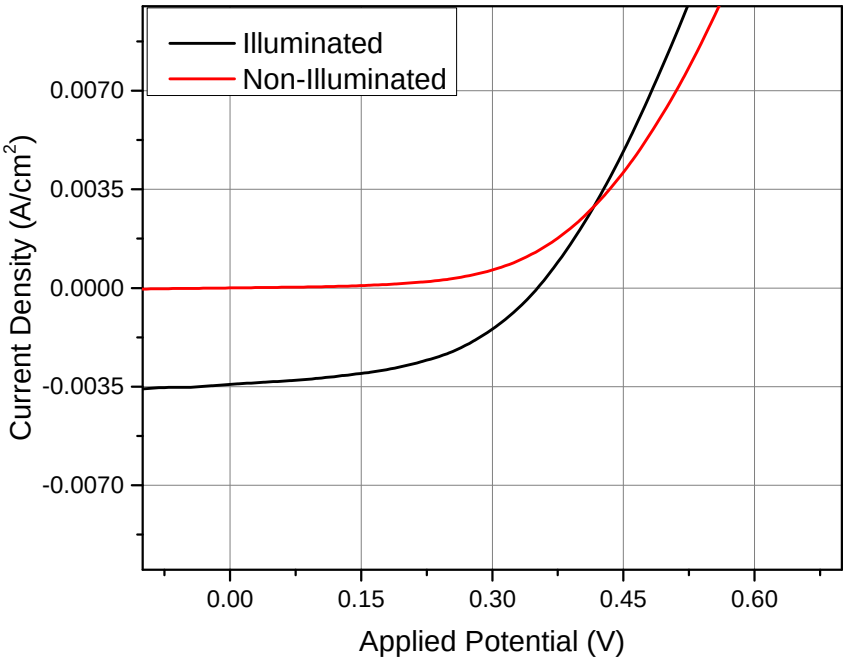

Figure 4.13: Current voltage plot of cell 140813_D1ML. Best device with the ITO/PEDOT:PSS/P3HT:PCBM/PFN/Al structure fabricated

occupied molecular orbitals facilitating hole transport toward PEDOT:PSS. Removing PEDOT:PSS the device, the active layer highest occupied molecular orbital remains lower than the valence band of the indium tin oxide however the energy levels are not well aligned, the lowest unoccupied molecular energy level is nearly equidistant from the valence band of indium tin oxide, as shown in Figure 4.14. Increased recombination of excitons at the indium tin oxide interface greatly reduces the short circuit current.

PEDOT:PSS re-enforces the organic material layers work function reducing the effect of indium tin oxide, which would shift the work function of the organic upward its own. The open circuit voltage of the ideal device at 0.5095V is less than the difference between aluminum and the PEDOT:PSS highest occupied molecular orbital, 0.9 V. Removing the PEDOT:PSS the work function is no longer re-enforced and indium tin oxide will likely control the work function at the interface. The difference between the work functions of indium tin oxide and aluminum is 0.4 V with a similar loss in open circuit voltage of 50% from the reference device taken into effect, the open circuit voltage of 0.2163 V is understandable.

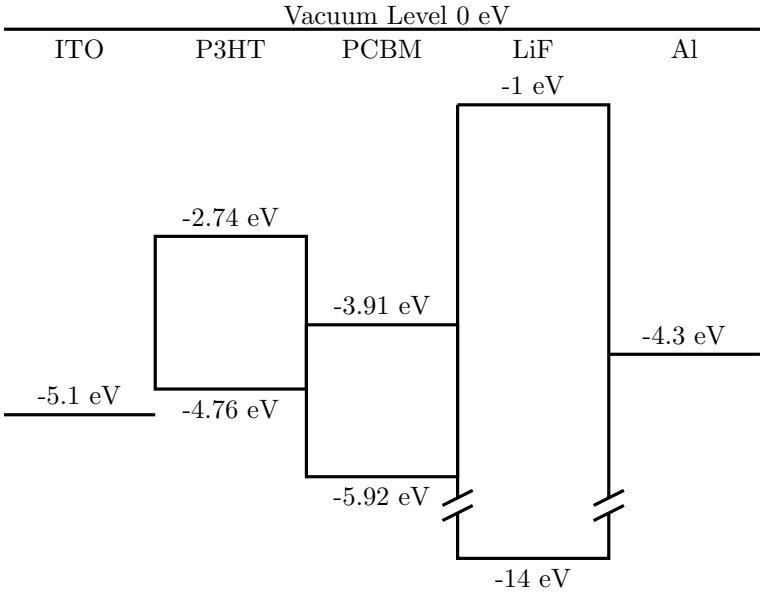

Figure 4.14: Energy level diagram for the removal of PEDOT:PSS

Cell ID	140611_D2BR	140827_D4ML	140813_D1ML	140807_D2BL
Voc (V)	0.5095	0.2100	0.3465	0.2163
Jsc (mA/cm^2)	-14.4	-3.16	-4.73	-3.91
Fill Factor (%)	44.0	41.4	50.2	38.4
Roc (Ohm cm^2)	11.6381	29.1173	23.4365	27.8858
Gsc (mS/cm^2)	21.5	39.5	23.3	40.0
Vmp (V)	0.3233	0.1252	0.2297	0.1264
Jmp (mA/cm^2)	-9.94	-2.19	-3.58	-2.57
PCE (%)	3.23	0.274	0.822	0.325

Table 4.5: Best Devices Characteristic Values

4.2 Inverted Devices

Inverting the direction of current flow in an organic device is achieved by changing the layers surrounding the active material. Given the core of the device one can choose the materials to produce a current flow in a desired direction. In this case the current flow of the device is typically toward the front of the device where the light enters. However, the direction of flow can be changed by simply switching the positions of the buffer layers employed in the device. By placing the electron transport layer at the front of the device and the hole transport layer at the back the direction of flow will be reversed, there are more considerations for the device to function in a meaningful fashion. There are several reasons one may wish to change the direction of current flow in a device, from exploiting the migration of charge carriers relative to the location in the device they are generated to enabling the usage of alternate materials to enable alternate device applications.

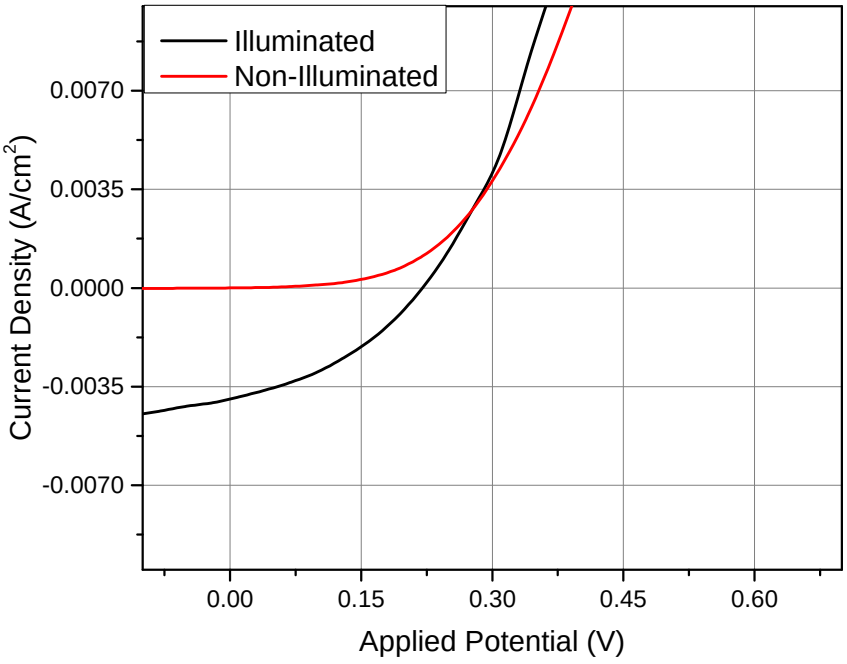

Figure 4.15: Current voltage plot of cell 140807_D2BL. Best device with the ITO/P3HT:PCBM/LiF/Al structure fabricated

The first step to inversion is choosing the buffer layer materials, previously the buffer layers consisted of PEDOT:PSS, lithium fluoride and PFN. Lithium fluoride deposition following the method employed previously will not work for this purpose as an additional shadow mask would need to be fabricated so it was decided to maintain solution processing for the front buffer layer. To accomplish this PFN was employed as the front buffer layer. PFN has been shown to modify the work function of materials that it coats raising the work function toward the vacuum level. This can be used to facilitate electron transport while hindering hole transport. PEDOT:PSS was chosen as the back buffer layer. There were complications with the deposition of PEDOT:PSS on the P3HT:PCBM active layer. The surface energy difference between the deposited active layer and the PEDOT:PSS solution was too great not allowing the PEDOT:PSS to coat the surface. Thus devices were fabricated with out a back buffer layer however they were not functional likely due to the reactivity of the aluminum, similar to the devices fabricate at the beginning of the project. Thanks to the assistance of John Purdy, the surface energy problem was overcome with the addition of a surfactant to the PEDOT:PSS solution, in this case soap. The soap allowed the PEDOT:PSS solution to coat the active layer surface resulting in functioning devices.

This is the best device fabricated using the device design shown in Figure 4.16, this design is the first in a

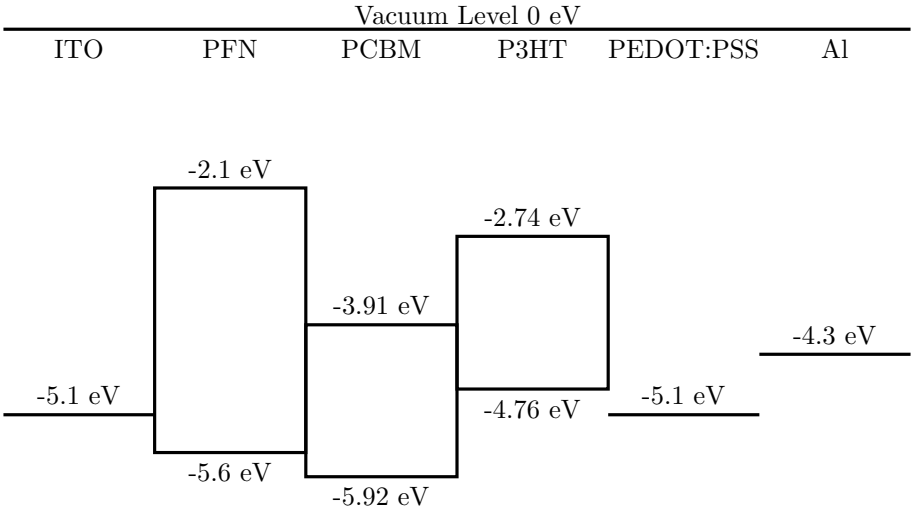

Figure 4.16: Energy level diagram for inverted device where PEDOT:PSS and PFN were switched to reverse current flow

series to refine the inverted device design. Comparing the illuminated and non-illuminated current response curves one can note the differing turn on potential, causing the curves to cross as seen in Figure 4.17. The non-illuminated device curve does not enter the on state of the diode long enough to compare the slope of the curves in the measured region of the device. The shift in turn on potential moves the open circuit voltage to a lower potential. Combined with the low short circuit current density the device efficiency is low at 0.178%. Table 4.6 shows the series resistance in the device is higher than higher efficiency regular devices reducing the fill factor to 36.9%, but the shunt resistance (short circuit conductance) is higher by an order of magnitude. Using this as a starting point the next change to device structure should focus on improving the open circuit voltage.

Gold was unsuccessful as a back contact in regular devices but the energy level alignment is favorable in an inverted structure, Figure 4.18. By employing gold as a back contact the potential difference between the gold back contact and the PFN modified work function at the front of the device is significantly larger than when aluminum is the back contact. This increases the open circuit voltage of the device from the 0.2875V with aluminum to 0.4727V with gold as the back contact. The larger innate potential in the device increases the short circuit current density. Both series resistance and shunt resistance in the device improve leading to a large increase in the power conversion efficiency, 0.861% shown in Table 4.6. The device curves still cross as in the previous device however the non-illuminated device turns on at a lower potential again the measured region of the curve does not include the linear region of the diode. Comparing this to the function of the regular devices this may point toward the device not functioning with its optimal open circuit

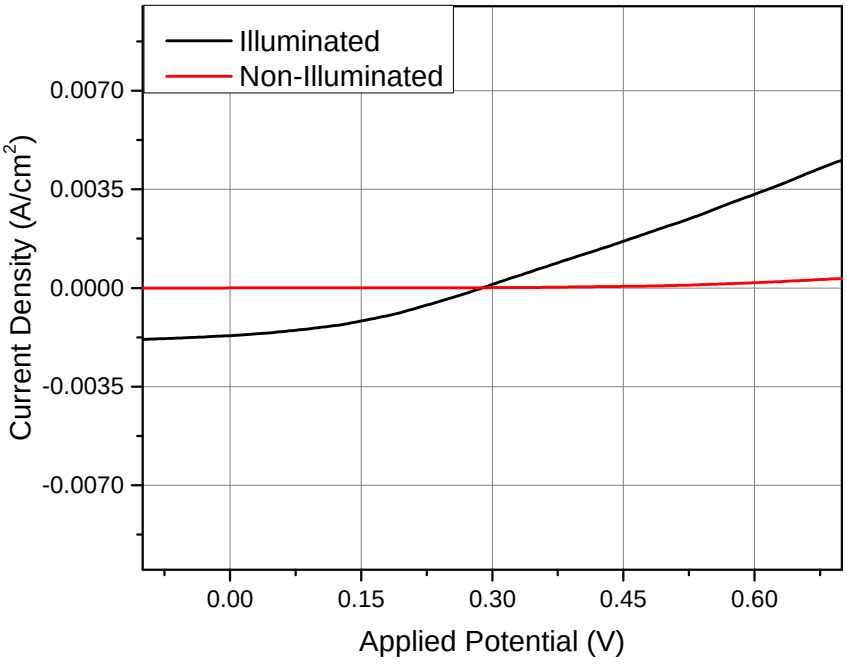

Figure 4.17: Current voltage plot of cell 140815_D1BR. Best device with the ITO/PFN/P3HT:PCBM/PEDOT:PSS/Al structure fabricated

voltage. The change from aluminum to gold back contact saw a significant change in the turn on of the non-illuminated device with the gold device having a lower turn on potential. The answer to this peculiar response to change may lay in possible secondary nonlinear current response nature of the device which is evident in between 0.45 and 0.75V. The secondary non-linear device mechanism is vertically aligned with the turn on of the non-illuminated device. This is very similar to what was seen in the first viable device, Figure 4.2. If the device function is significantly impaired then there is room for device design improvement, likely in refinement of charge carrier movement control through the use of alternate buffer materials or additional buffer layers. The aluminum contacted device may show a similar effect however it is less evident.

The electrical characteristics of the PEDOT:PSS utilized in the inverted structure is an unknown given the use of a surfactant to enable coating of the active layer. Changes in the PEDOT:PSS film may cause the initial non-linear current response that leads to early turn on of the device reducing the power generation region. Removing the PEDOT:PSS layer is expected o significantly restrict device function, as seen when aluminum was the back contact however gold is much less reactive than aluminum. Gold deposition directly on the active layer yields devices that function better than devices with the surfactant modified PEDOT:PSS buffer layer. The device curves in Figure 4.21 show a well defined power generation region with a fill factor

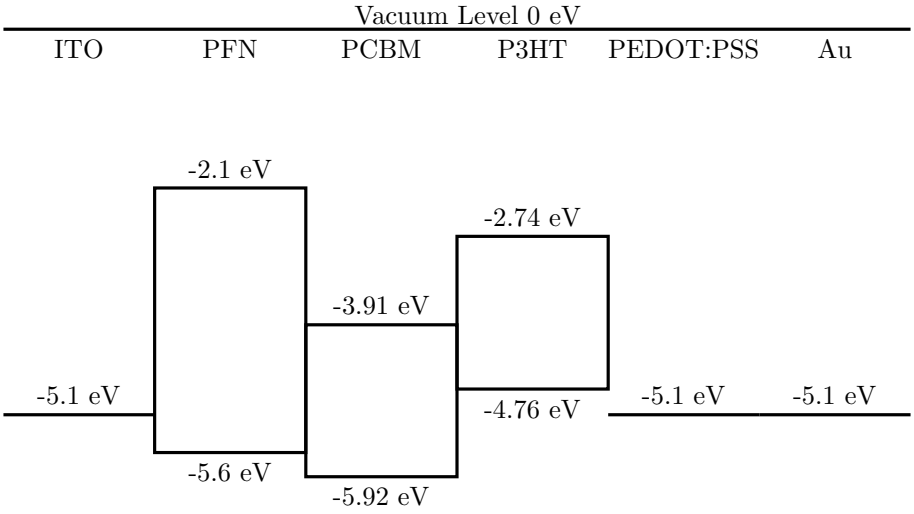

Figure 4.18: Energy level diagram for inverted device where aluminum is replaced with gold to reverse increase the open circuit voltage

of 47.1% and a power conversion efficiency of 0.912%. Series resistance is reduced by half compared to the device that included PEDOT:PSS with soap, but the short circuit conductance is higher thus the shunt resistance is lower. The greatest change in the device is seen in the series resistance and how that affects the on state of the device. There are still two non-linear current response mechanisms at work in the device with the second mechanism appearing in the same region of the plot. The cause of the initial mechanism requires further investigation, using the regular devices as a reference if this issue were resolved the open circuit of the devices could rise to between 0.7V and 1V. This would mark a significant improvement in device function with a large improvement in power conversion efficiency.

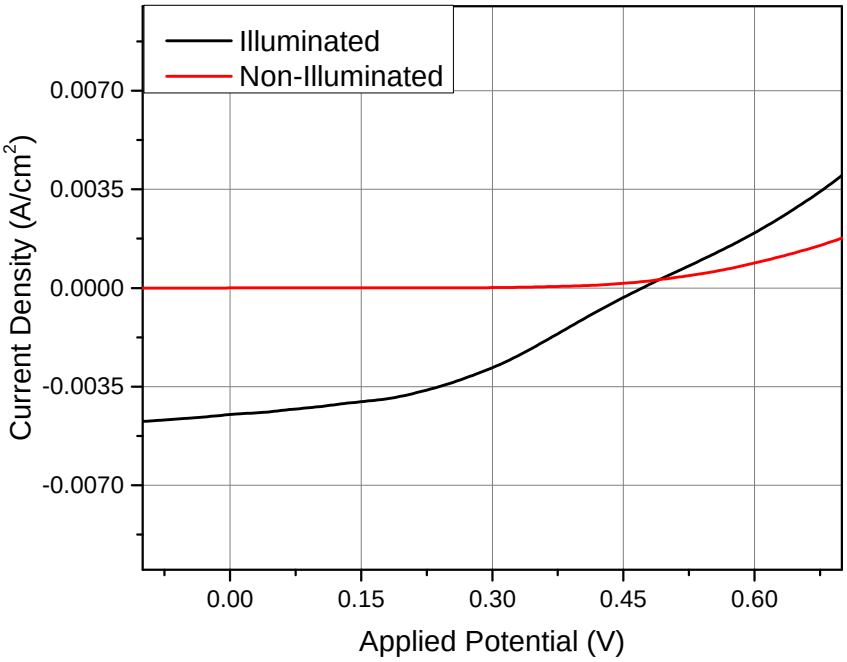

Figure 4.19: Current voltage plot of cell 140819_D2MR. Best device with the ITO/PFN/P3HT:PCBM/PEDOT:PSS/Au structure fabricated

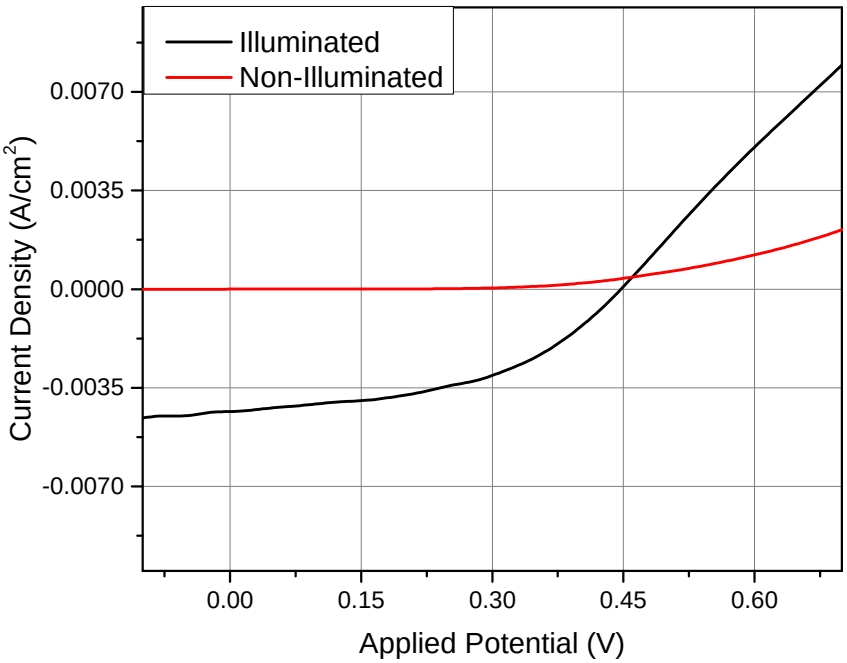

Figure 4.21: Current voltage plot of cell 140819_D4BR. Best device with the ITO/PFN/P3HT:PCBM/Au structure fabricated

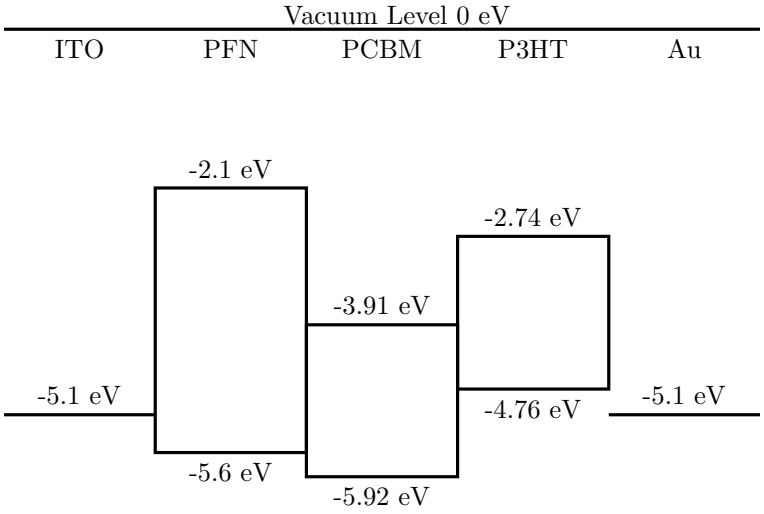

Figure 4.20: Energy level diagram for inverted device where PEDOT:PSS was removed to investigate its contribution to device function in an inverted structure

Cell ID	140815_D1BR	140819_D2MR	140819_D4BR
Voc (V)	0.2875	0.4727	0.4453
Jsc (mA/cm^2)	-1.68	-4.50	-4.34
Fill Factor (%)	36.9	40.6	47.1
Roc (Ohm cm^2)	97.8714	65.6887	31.9774
Gsc (mS/cm^2)	5.12	6.70	8.42
Vmp (V)	0.1619	0.2718	0.2960
Jmp (mA/cm^2)	-1.10	-3.18	-3.08
PCE (%)	0.178	0.864	0.912

Table 4.6: Best Inverted Devices Characteristic Values

4.3 Short Life Time Testing

Testing the effects of exposing photo-voltaic devices to sunlight is essential to determining the viability of a device in a power generation application. There are various changes that can occur within the device that will affect different aspects of the performance. Through short lifetime testing, over a 105 minute period sampling in 15 minute intervals, there were two opposing trends. The highest performing device prior to exposure to simulated sun light degraded while the lowest performing device improved through exposure. Investigating the parameters that are effected will point toward the nature of the change in the device.

The best performing device prior to extended exposure to simulated solar emission is the same best preforming device with the indium tin oxide, PEDOT:PSS, P3HT:PCBM, lithium fluoride, and aluminum structure. Table 4.7 shows the change in characteristic values over the short life time testing of the best

performing device prior to extended exposure to simulated solar irradiation. The power conversion efficiency of the device started at 3.23% dropping to 2.45% after 105 minutes. The drop in efficiency is not linear, there is a sharp drop in efficiency after 15 minutes with the device dropping to 1.39% power conversion efficiency. However, the efficiency is not stable with the efficiency at 30 minutes coming back up to 2.62% but dropping again at 45 minutes to 1.69%. The efficiency stabilizes in a downward trend from 45 minutes to 75 minutes then increases from 90 minutes to 105 minutes. A similar trend is seen in most of the other devices, with the exception of the lowest efficiency devices.

Efficiency is governed by several factors that can change if the device structure is modified under solar irradiation. The first notable change expected is the morphology of the active material. Phase segregation in the active layer through Oswald ripening leads to a growth of the domain sizes of the individual materials that make up the absorbing layer. Once the domain sizes grow too large there is an increase in recombination effects seen in the shunt resistance, and short circuit current. Short circuit current follows a similar trend to that of the power conversion efficiency, with shunt resistance having an opposite response as expected. Changes in domain sizes will also affect the mobility of charge carriers in the material, seen in the series resistance of the device. The open circuit voltage varies slightly with the changes in series resistance however the change is small. Fill factor tells an interesting tale with an increase initially that corresponds with a reduction in efficiency indicating resistances are not the largest contributors to efficiency drop until after 15 minutes. After the 60 minute mark the fill factor continues to drop through the testing period. The largest change is the short circuit current causing the large drop in efficiency initially then the resistance contributes to reduce the fill factor resulting in the overall reduction in efficiency. Changes in resistance can also be attributed to chemical degradation of the device. Oxidation of materials tends to increase the band gap of materials making a semiconducting material insulating, increasing in the device resistance. The incident solar irradiation provides the necessary activation energy for changes in chemical structure. Given that devices that have been in the testing room, not exposed to sunlight are no longer functional after a couple of months. The encapsulation of the devices is imperfect but limiting the exposure to atmospheric conditions.

Exposure Time (Minutes)	Voc (V)	Jsc (mA/cm^2)	Fill Factor (%)	Roc (Ω cm^2)	Gsc (mS/cm^2)	PCE (%)
0	0.5095	-14.4	44.0	11.6381	21.5	3.23
15	0.4800	-6.46	44.9	21.6700	13.3	1.39
30	0.5073	-14.8	34.8	17.0650	21.3	2.62
45	0.4898	-9.00	38.3	22.8580	15.2	1.69
60	0.4874	-8.29	39.0	23.8928	14.4	1.57
75	0.4873	-8.15	39.0	24.2736	14.1	1.55
90	0.5036	-14.7	32.7	18.6531	21.2	2.43
105	0.5082	-13.9	34.6	18.9007	19.9	2.45

Table 4.7: Best preforming device prior to short lifetime testing characteristic values

Starting with a low efficiency device the short life time testing improved the device efficiency. Table 4.8 displays the characteristic values for the least efficient device prior to exposure to simulated solar irradiation. The device efficiency increases rapidly initially, the improvement levels off which is the opposite response seen in the highest efficiency device. The highest efficiency of the device occurs after 45 minutes reaching 0.757%, corresponding with a rise in the short circuit current and increase in fill factor. This device shows improvement in several areas however the most significant would seem to be the open circuit voltage. The open circuit voltage also increases significantly initially but reaches a maximum of 0.5125V at 75 minutes. At 105 minutes the power conversion efficiency is 0.712% with a relatively high open circuit voltage and short circuit current for the device. Short circuit current fluctuates but does not see a significant improvement. Shunt resistance is significantly reduced after 15 minutes of exposure and stabilizes, with only minor variations after 15 minutes. Series resistance is reduced after exposure but the difference is only 30Ω and at 105 minutes the difference is only 12Ω. Changes in morphology can correct defects in films thereby reducing shunt currents improving the open circuit voltage. Examination of the initial current response curve one can note inconsistencies in the illuminated curve that are not present in future tests. Inconsistencies in device curves that are not present in future tests indicate alternate current pathways that are unstable, and break down when operating. The non-illuminated current response also shows inconsistencies that are smoothed out in future tests.

This device is on the same substrate as a device with an efficiency of 3.10%

Exposure Time (Minutes)	Voc (V)	Jsc (mA/cm^2)	Fill Factor (%)	Roc (Ω cm^2)	Gsc (mS/cm^2)	PCE (%)
0	0.3560	-4.18	14.0	71.1466	17.3	0.209
15	0.4887	-3.75	32.9	71.4398	6.45	0.604
30	0.4925	-4.96	30.8	68.8641	7.87	0.750
45	0.4985	-5.17	29.3	73.4170	7.76	0.757
60	0.4880	-4.80	28.3	87.1399	7.77	0.662
75	0.5125	-4.03	32.7	60.7317	6.31	0.676
90	0.4069	-4.02	37.5	41.2961	7.28	0.615
105	0.5114	-4.80	29.0	59.8028	7.31	0.712

Table 4.8: Worst preforming device prior to short lifetime testing characteristic values

Chapter 5

Summary

Starting from the Ossila fabrication guide and various theses for guidance initial devices were fabricated. Devices have a planar structure utilizing: indium tin oxide as a transparent front contact, PEDOT:PSS as a hole transport front buffer layer, P3HT:PCBM as the absorbing bulk heterojunction, and an aluminum back contact. Device function was improved by reducing the interaction between aluminum and the absorbing layer, using a lithium fluoride as an electron tunnel back buffer layer, that also inhibited the flow of holes toward the aluminum back layer. This combination reduced the unwanted nonlinear current response likely from a metal insulator metal device function as characterized by the symmetric current response in either direction, by controlling the flow of charge carriers. Further device refinement came when the indium tin oxide coated glass slide substrates were replaced with patterned indium tin oxide substrates. The substitution controlled the cell area reducing the effect of individual defects on device function, and moved the electrical contacts to the side of the device to reduce the probability of mechanical degradation of devices during testing. Ossila patterned substrates also provided a reliable encapsulation method to improve the endurance of devices by reducing the atmospheric interaction of completed devices. During this process three essential insights in device fabrication were learned cleaning, fabrication speed, and quantity. Cleaning is the most important part of the solution fabrication process, imperfections on the substrate will create defects that cause the entire device to fail. Fabrication speed reduces the time that sensitive organic materials are exposed to atmosphere, by becoming familiar with the fabrication process device yield is improved. By fabricating a greater number of devices increases the probability of producing a high functioning device, reducing the effect of defects on device yield. There is a balance between quantity of devices fabricated and the time required to fabricate the devices, balancing the two improves device yield significantly. Optimization of the active and front buffer layers proved impractical as variation in device function did not allow for conclusive determination of optimal coating speed. This could be a case where quantity of devices reduced fabrication speed to a point where atmospheric interaction was significant.

Properties of individual device structures and materials were investigated to compare expected characteristics to reality. The first alteration was the back contact replacing aluminum with gold. The work function

of gold is much lower than that of aluminum, in the current structure the front electrode is the anode and rear electrode is the cathode. With gold having a lower work function, the difference between the work function of the front and back electrodes is significantly reduced, reducing the open circuit voltage as expected from theory. Short circuit current density is reduced due to the reduced potential across the device. In an attempt to improve series resistance in the device the lithium fluoride back buffer layer was replaced with PFN. PFN is an electron transport material that has been shown to raise the work function at the interface of materials coated by up to 2 eV. The series and shunt resistances of the device were not significantly improved, however the fill factor increased to 50.2% from 44.0%. Testing the properties of the front buffer layer was performed by removing the PEDOT:PSS layer from the device. PEDOT:PSS is intended to smooth the rough indium tin oxide surface and selectively transport holes. Removal of the layer required extra attention to cleaning in the fabrication process to evenly coat the indium tin oxide surface with the absorbing material. The open circuit voltage of the device dropped because the control of charge carrier movement was reduced as excited electrons were no longer blocked from interacting with the front contact.

Changing the direction of current flow in an organic diode structure is as simple as switching the buffer layers. Exchanging PEDOT:PSS with PFN an inverted device can be fabricated. Deposition of PEDOT:PSS on top of the active layer required the addition of a surfactant to overcome the surface energy mismatch, the surfactant allows the PEDOT:PSS to coat the surface by providing two dissimilar ends one for each material, one hydrophilic and the other hydrophobic. The first devices had the following structure indium tin oxide, PFN, P3HT:PCBM, PEDOT:PSS, and aluminum. This device displayed a low open circuit voltage as expected due to the high work function aluminum used as the anode. Replacing aluminum with gold the open circuit voltage improved significantly raising the power conversion efficiency from 0.2875% with aluminum to 0.864% with gold. The electrical properties of the modified PEDOT:PSS are unknown so a set of devices were fabricated without the PEDOT:PSS back buffer layer. A device in the set without a back buffer layer displayed the highest power conversion efficiency of all inverted devices fabricated at 0.912%. The inverted device current response curves show two non-linear current responses with the first turning on under illumination before the desired turn on potential of the non-illuminated curve. Indicating the possibility of increasing the open circuit voltage from 0.4453V to between 0.7V and 1V, through the use of alternate or additional buffer layers to better control the movement of charge carriers.

Short lifetime tests were preformed to examine changes in device function over a short period of time under simulated solar irradiation. Devices are expected to be annealed by excess energy many photons will contribute during absorption. Annealing is expected to increase device performance initially with performance falling off over time as domains within the bulk heterojunction grow through Oswald ripening. Both of these effects were observed simultaneously in different devices, with the highest performing devices degrading

initially and lowest performing devices improving. Annealing explains most of the changes seen in the best preforming device. The lowest performing device experiences a different change through the elimination of shunt current pathways during the first test caused by the current passing through the device and changes in the morphology due to annealing greatly improving the open circuit voltage. There is a significant amount of variation in device performance even on a single substrate with devices ranging from 0.209% to 3.11% power conversion efficiency. After prolonged exposure to simulated solar irradiation the device performance across a substrate tends to converge with high performance devices degrading and low performing devices improving.

This project has laid the ground work for future projects that utilize alternate active materials. Devices are not limited to photovoltaic devices the diode structure used here can be applied to organic light emitting diodes.

5.1 Future work

There are many directions this project could move in the future from testing alternate materials in the various parts of the structure to alternate device functions through changing the active material.

I would suggest a movement towards complete solution processed devices as the main benefit for organic devices lies in the easy and cost effective fabrication. Moving from a physical vapor deposited back contact material to a solution processed back contact would reduce fabrication time and equipment cost significantly.

One could also move towards flexible devices by replacing the brittle indium tin oxide transparent conducting oxide. The key to flexibility seems to be in a movement away from crystalline oxide materials and toward either conducting polymers or large scale flexible lattice systems such as graphene. For optical devices the conductivity of the material and the transparency must be balanced to maintain reasonable functionality.

Buffer layers are essential to manipulation of device function. Exploration of alternate materials that can optimize a device function is essential to the future of organic electronics. With new materials fabricated all the time proper characterization of the electronic properties is a never ending, in the pursuit of better device function.

Similarly absorbing materials are the basis of any photovoltaic device. Improving absorption while maintaining the ability to disassociate charge carriers and produce power will remain the leading aspect of device research. The progress in absorbing materials is progressing at an amazing rate with hybrid organic systems reaching 20% power conversion efficiency.

Limiting factors of the performance of devices must not be overlooked with alternate technologies showing great promise. Rectifying antennas have been theorized to have a power conversion efficiency of 90% of a

monochromatic wavelength. Breaking through barriers imposed by current device structure must not be overlooked in the pursuit of high efficiency renewable power generation.

References

[1] N.S. Sariciftci and S.S. Sun. *Organic Photovoltaics: Mechanism, Materials, and Devices.* Taylor & Francis New York, 2005.

[2] A. Köhler and H. Bässler. *Electronic Processes in Organic Semiconductors: An Introduction.* John Wiley & Sons, 2015.

[3] B. Wunderlich. A classification of molecules, phases, and transitions as recognized by thermal analysis. *Thermochimica Acta*, 340:37–52, 1999.

[4] S.I. Na, B.K. Yu, S.S. Kim, D. Vak, T.S. Kim, J.S. Yeo, and D.Y. Kim. Fully spray-coated ito-free organic solar cells for low-cost power generation. *Solar Energy Materials and Solar Cells*, 94:1333–1337, 2010.

[5] I. Jeon, C. Delacou, A. Kaskela, E.I. Kauppinen, S. Maruyama, and Y. Matsuo. Metal-electrode-free window-like organic solar cells with p-doped carbon nanotube thin-film electrodes. *Scientific Reports*, 6:31348, 2016.

[6] H.O. Pierson. *Handbook of carbon, graphite, diamonds and fullerenes: processing, properties and applications.* William Andrew, 2012.

[7] J.D. Roberts and M.C. Caserio. *Basic principles of organic chemistry.* WA Benjamin, Inc., 1977.

[8] N. Grossiord, J.M. Kroon, R. Andriessen, and P.W.M. Blom. Degradation mechanisms in organic photovoltaic devices. *Organic Electronics*, 13:432–456, 2012.

[9] I. Clover. Organic electronics market to be worth $79.6 billion by 2020. Retreived from `http://www.pv-magazine.com/news/details/beitrag/organic-electronics-market-to-be-worth-796-billion-by-2020_100016825/#axzz4NwI7AkFw`, 2014.

[10] S.R. Forrest. The path to ubiquitous and low-cost organic electronic appliances on plastic. *Nature*, 428:911–918, 2004.

[11] S.E. Habas, H.A.S. Platt, M.F.A.M. Van Hest, and D.S. Ginley. Low-cost inorganic solar cells: from ink to printed device. *Chemical Reviews*, 110:6571–6594, 2010.

[12] National Energy Board. Canada's energy future 2016: Energy supply and demand projections to 2040. Retreived from `www.neb-one.gc.ca/energyfutures`, 2016.

[13] M.B. McElroy. *Energy: Perspectives, Problems, and Prospects.* OUP USA, 2010.

[14] C. Morris and M. Pehnt. Energy transition: The german energiewende. Retreived from `www.energytransition.de`, 2012.

[15] A. Aslani, M. Naaranoja, and K.V. Wong. Strategic analysis of diffusion of renewable energy in the Nordic countries. *Renewable and Sustainable Energy Reviews*, 22:497–505, 2013.

[16] W. A. Hermann. Quantifying global exergy resources. *Energy*, 31:1685–1702, 2006.

[17] R.N. Marks, J.J.M. Halls, D.D.C. Bradley, R.H. Friend, and A.B. Holmes. The photovoltaic response in poly (p-phenylene vinylene) thin-film devices. *Journal of Physics: Condensed Matter*, 6:1379, 1994.

[18] NREL. Best research-cell efficiencies. Retrieved from http://www.nrel.gov/ncpv/images/efficiency_chart.jpg, 2016.

[19] R. Dick. *Advanced Quantum Mechanics: Materials and Photons*. Graduate Texts in Physics. Springer New York, 2012.

[20] S.O. Kasap. *Principles of electronic materials and devices*. McGraw-Hill, 2006.

[21] J.A. Key and D.W. Ball. Introductory chemistry-1st canadian edition. Retreived from https://opentextbc.ca/introductorychemistry/, 2014.

[22] R.E. Merrifield. Exciton multiplicities. *The Journal of Chemical Physics*, 23:402–402, 1955.

[23] D.J. Griffiths. *Introduction to quantum mechanics*. Pearson Prentice Hall, 2005.

[24] M A Baldo, D F O'Brien, M E Thompson, and S R Forrest. Excitonic singlet-triplet ratio in a semiconducting organic thin film. *Physical Review B*, 60:14422–14428, 1999.

[25] R.R. Lunt, N.C. Giebink, A.A. Belak, J.B. Benziger, and S.R. Forrest. Exciton diffusion lengths of organic semiconductor thin films measured by spectrally resolved photoluminescence quenching. *Journal of Applied Physics*, 105:053711, 2009.

[26] J. Singh. Radiative recombination and lifetime of a triplet excitation mediated by spin-orbit coupling in amorphous semiconductors. *Physical Review B*, 76:085205, 2007.

[27] D.L. Dexter. A theory of sensitized luminescence in solids. *The Journal of Chemical Physics*, 21:836–850, 1953.

[28] T. Förster. 10th spiers memorial lecture. transfer mechanisms of electronic excitation. *Discussions of the Faraday Society*, 27:7–17, 1959.

[29] S.H. Lin, W.Z. Xiao, and W. Dietz. Generalized förster-dexter theory of photoinduced intramolecular energy transfer. *Physical Review E*, 47:3698–3706, 1993.

[30] P. Stallinga. Electronic transport in organic materials: Comparison of band theory with percolation/(variable range) hopping theory. *Advanced Materials*, 23:3356–3362, 2011.

[31] G.B. Rybicki and A.P. Lightman. *Radiative processes in astrophysics*. John Wiley & Sons, 2008.

[32] D.R. Willims. Sun fact sheet. Retreived from http://nssdc.gsfc.nasa.gov/planetary/factsheet/sunfact.html, 2016.

[33] C. Wehrli. Extraterrestrial solar spectrum. *Chemical Reviews*, 615:6571–6594, 1985.

[34] ASTM. Standard solar constant and zero air mass solar spectral irradiance tables. Retreived from http://www.astm.org/Standards/E490.htm, 2000.

[35] NREL. Solar spectra: Air mass zero. Retreived from http://rredc.nrel.gov/solar/spectra/am0/.

[36] C. Gueymard. *SMARTS2: a simple model of the atmospheric radiative transfer of sunshine: algorithms and performance assessment*. Florida Solar Energy Center Cocoa, FL, 1995.

[37] C.A. Gueymard. Parameterized transmittance model for direct beam and circumsolar spectral irradiance. *Solar Energy*, 71:325–346, 2001.

[38] ASTM. Standard tables for reference solar spectral irradiances: Direct normal and hemispherical on 37^o tilted surface. Retreived from http://www.astm.org/Standards/G173.htm, 2012.

[39] NREL. Reference solar spectral irradiance: Air mass 1.5. Retreived from http://rredc.nrel.gov/solar/spectra/am1.5/.

[40] S.R. Wenham, M.A. Green, M.E. Watt, R.P. Corkish, and A.B. Sproul. *Applied photovoltaics*. Earthscan, 2011.

[41] Daniel A Steck. Classical and modern optics. Availible online `http://steck.us/teaching`, 2015.

[42] M. Balkanski and R.F. Wallis. *Semiconductor physics and applications*. Oxford University Press, 2000.

[43] J.J. Sakurai. *Modern quantum mechanics*. Addison-Wesley, 1994.

[44] T.R. Kuphaldt. Lessons in electric circuits, volume iii–semiconductors. *Vol. Fifth Edition. Open Book Project*, 2009.

[45] C.S. Solanki. *Solar photovoltaics: fundamentals, technologies and applications*. PHI Learning Pvt. Ltd., 2015.

[46] J.C. Bernede. Organic photovoltaic cells: history, principle and techniques. *Journal of the Chilean Chemical Society*, 53:1549–1564, 2008.

[47] Y. Tamai, H. Ohkita, H. Benten, and S. Ito. Exciton diffusion in conjugated polymers: From fundamental understanding to improvement in photovoltaic conversion efficiency. *The Journal of Physical Chemistry Letters*, 6:3417–3428, 2015.

[48] F.H. Schacher, P.A. Rupar, and I. Manners. Functional block copolymers: nanostructured materials with emerging applications. *Angewandte Chemie International Edition*, 51:7898–7921, 2012.

[49] C. Grieco, M.P. Aplan, A. Rimshaw, Y. Lee, T.P. Le, W. Zhang, Q. Wang, S.T. Milner, E.D. Gomez, and J.B. Asbury. Molecular rectification in conjugated block copolymer photovoltaics. *The Journal of Physical Chemistry C*, 120:6978–6988, 2016.

[50] E. Verploegen, R. Mondal, C.J. Bettinger, S. Sok, M.F. Toney, and Z. Bao. Effects of thermal annealing upon the morphology of polymer–fullerene blends. *Advanced Functional Materials*, 20:3519–3529, 2010.

[51] B. Ray, P.R. Nair, and M.A. Alam. Annealing dependent performance of organic bulk-heterojunction solar cells: A theoretical perspective. *Solar Energy Materials and Solar Cells*, 95:3287–3294, 2011.

[52] N. Rastogi and N. Singh. Optical simulation of organic photovoltaic device, 2016.

[53] Q. Li, W.J. Yoon, and H. Ju. Optimization of an organic photovoltaic device via modulation of thickness of photoactive and optical spacer layers. *Nanoscale Research Letters*, 9:1, 2014.

[54] X. Guo, X. Liu, F. Lin, H. Li, Y. Fan, and N. Zhang. Highly conductive transparent organic electrodes with multilayer structures for rigid and flexible optoelectronics. *Scientific Reports*, 5:10569, 2015.

[55] D. Angmo and F.C. Krebs. Flexible ito-free polymer solar cells. *Journal of Applied Polymer Science*, 129:1–14, 2013.

[56] K.B. Kim, Y.H. Tak, Y.S. Han, K.H. Baik, M.H. Yoon, and M.H. Lee. Relationship between surface roughness of indium tin oxide and leakage current of organic light-emitting diode. *Japanese Journal of Applied Physics*, 42:L438, 2003.

[57] R. Po, C. Carbonera, A. Bernardi, and N. Camaioni. The role of buffer layers in polymer solar cells. *Energy & Environmental Science*, 4:285–310, 2011.

[58] K. Wang, C. Liu, T. Meng, C. Yi, and X. Gong. Inverted organic photovoltaic cells. *Chemical Society Reviews*, 45:2937–2975, 2016.

[59] S. Lattante. Electron and hole transport layers: their use in inverted bulk heterojunction polymer solar cells. *Electronics*, 3:132–164, 2014.

[60] M. Morsli, J.C. Bernède, L. Cattin, F. Dahou, and A. Khelil. On the exciton blocking layer at the interface organic/cathode in multiheterojunction organic solar cells. *Energy Procedia*, 31:74–80, 2012.

[61] A. Cheknane, H.S. Hilal, F. Djeffal, B. Benyoucef, and J.P. Charles. An equivalent circuit approach to organic solar cell modelling. *Microelectronics Journal*, 39:1173–1180, 2008.

[62] W. Shockley and H.J. Queisser. Detailed balance limit of efficiency of p-n junction solar cells. *Journal of applied physics*, 32:510–519, 1961.

[63] L.C. Hirst and N.J. Ekins-Daukes. Fundamental losses in solar cells. *Progress in Photovoltaics: Research and Applications*, 19:286–293, 2011.

[64] S.J. Byrnes. The shockley-queisser limit. availible online `http://sjbyrnes.com/sq.html`, 2016.

[65] M. Jørgensen, K. Norrman, and F.C Krebs. Stability/degradation of polymer solar cells. *Solar Energy Materials and Solar Cells*, 92:686–714, 2008.

[66] J.H. Yao, K.R. Elder, H. Guo, and M. Grant. Theory and simulation of ostwald ripening. *Physical Review B*, 47:14110, 1993.

[67] B. Conings, S. Bertho, K. Vandewal, A. Senes, J. D'Haen, J. Manca, and R.A.J. Janssen. Modeling the temperature induced degradation kinetics of the short circuit current in organic bulk heterojunction solar cells. *Applied Physics Letters*, 96:163301, 2010.

[68] Ossila Ltd. The ossila organic photovoltaic (opv) and organic light emitting diode (oled) fabrication manual. Retrieved 7 February 2013 from `www.ossila.com`.

[69] Ossila Ltd. Organic photovoltaic (opv) and organic light emitting diode (oled) fabrication manual. Retrieved from `www.ossila.com`.

[70] H.L. Yip and Alex K.Y. Jen. Recent advances in solution-processed interfacial materials for efficient and stable polymer solar cells. *Energy & Environmental Science*, 5(3):5994, 2012.

[71] J.J. van Franeker, W.P. Voorthuijzen, H. Gorter, K.H. Hendriks, R.A.J. Janssen, A. Hadipour, R. Andriessen, and Y. Galagan. All-solution-processed organic solar cells with conventional architecture. *Solar Energy Materials and Solar Cells*, 117:267–272, 2013.

[72] Z. He, C. Zhong, S. Su, M. Xu, H. Wu, and Y. Cao. Enhanced power-conversion efficiency in polymer solar cells using an inverted device structure. *Nature Photonics*, 6:591–595, 2012.

[73] Ossila Ltd. Pfn: Fabrication routine. Retrieved from `https://www.ossila.com/products/pfn`.

[74] Ossila Ltd. Ito substrates for oleds (pixelated anode): Datasheet. Retrieved from `https://www.ossila.com/products/oled-ito-substrates`.

[75] Y. Kim. Power-law-type electron injection through lithium fluoride nanolayers in phosphorescence organic light-emitting devices. *Nanotechnology*, 19:355207, 2008.

[76] Cost Effective Equiptment. Spin coat theory.

[77] Z. Zhong, Y. Zhong, C. Liu, S. Yin, W. Zhang, and D. Shi. Study on the surface wetting properties of treated indium-tin-oxide anodes for polymer electroluminescent devices. *Physica Status Solidi (A)*, 198:197–203, 2003.

[78] T. Kobayashi, H. Yamaguchi, and T. Nakada. Effects of combined heat and light soaking on device performance of cu (in, ga) se2 solar cells with zns (o, oh) buffer layer. *Progress in Photovoltaics: Research and Applications*, 22:115–121, 2014.